Project title	Safe, Efficient and Autonomous: Multimodal Library of European Shortsea and inland Solutions		
Project acronym	SEAMLESS		
Project number	101096923		
Project start date	01/01/2023	**Duration**	48 months

D4. 2 - AUTONOMOUS GNC SCHEME DEVELOPMENT AND MONITORING AGENT PROTOTYPE

Due date	30/12/2025	**Delivery date**	01/14/2026
Work package	WP4		
Responsible Author(s)	Nikos Kougiatsos (TU Delft), Vasso Reppa (TU Delft)		
Contributor(s)			
Reviewer(s)	Reda Yaich (IRTSX), Håvard Nordahl (SINTEF Ocean), Renan Guedes Maidana (SINTEF Ocean)		
Version	1.0		
Dissemination level	Public		

VERSION AND AMENDMENTS HISTORY

Version	Date (MM/DD/YYYY)	Created/Amended by	Changes
0.10	11/21/2025	Nikos Kougiatsos (TUD)	First draft, ready for review
0.20	12/12/2025	Reda Yaich (IRTSX), Håvard Nordahl (SINTEF Ocean), Renan Guedes Maidana (SINTEF Ocean)	Internal Review by consortium
1.00	01/14/2026	Nikos Kougiatsos (TUD), Vasso Reppa (TUD)	Ready for Submission

Funded by the European Union

Funded by the European Union. Views and opinions expressed are however those of the author(s) only and do not necessarily reflect those of the European Union or CINEA. Neither the European Union nor CINEA can be held responsible for them. Grant Agreement N° 101096923.

REFERENCES TO THIS DOCUMENT – ACKNOWLEDGMENTS

The material in this publication can be reproduced provided that a proper reference is made to the title of this publication and to the SEAMLESS project (https://www.seamless-project.eu). References to this document should use the following format, modified as appropriate to the publication where the reference appears:

Kougiatsos, Nikos; Reppa V.: "SEAMLESS deliverable D4.2: Autonomous GNC Scheme development and monitoring agent prototype", January 2026

The authors listed in the above citation have contributed material that has been included (more or less) verbatim in this report. The editor and contributors also acknowledge all other comments and inputs to this document from all participants in the SEAMLESS project.

Funded by the European Union

Funded by the European Union. Views and opinions expressed are however those of the author(s) only and do not necessarily reflect those of the European Union or CINEA. Neither the European Union nor CINEA can be held responsible for them. Grant Agreement N° 101096923.

EXECUTIVE SUMMARY

The SEAMLESS project aims to develop and adapt missing building blocks and enablers into a fully automated, economically viable, cost-effective, and resilient waterborne freight feeder loop service for Short Sea Shipping (SSS) and Inland Waterway Transport (IWT). The development of Building Block #2: “Modular vessel and operations concepts” is the main focus of Work Package 4.

Deliverable D4.2 – “Autonomous GNC Scheme development and monitoring agent prototype” is based on the research carried out in the context of Task 4.2 – “Development of Autonomous vessels GNC scheme”. Delft University of Technology is the leader of Task 4.2, with other participating partners being IRTSX, SO, NTUA, and NTNU. The task description in the Grant Agreement (GA) is as follows:

“This task will develop a GNC scheme for SSS and IWT autonomous vessels, exploiting precise positioning (i.e., Galileo/EGOS) which will be: 1) COLREG-compliant for safe navigation within waterways with mixed traffic, and 2) fault-tolerant for contributing towards reducing redundancy requirements. COLREG-compliance will be achieved by exploring the capability to express regulations with a suitable mathematical representation and deriving requirements for sensors, including water depth sensors (e.g., sonars) or lidars/cameras to avoid collision with spatial boundaries (where the GNSS measurements are not accurate). In addition, the effect of COLREGs alterations on this predicament, will be explored. Fault-tolerance will be implemented through the development of a monitoring module capable of: (i) detecting local fault occurrence, (ii) isolating the fault type (e.g. sensor fault, engine fault) and/or location (e.g. radar sensor fault, GNSS sensor fault), (iii) distinguishing between local faults and falsified communicated data (e.g. spoofing of AIS data) and propagated faults, and (iv) managing remedial actions (e.g. by reconstructing the faulty sensor information using virtual sensors, or by using virtual actuators to reconstruct the actions, or by adapting the controller). Analytical redundancy (e.g., quantitative, and qualitative models of the vessels and their components) will be utilized to develop the fault diagnosis and fault management techniques.”

This deliverable presents the development of two key components within the SEAMLESS project’s Work Package 4: the traffic rule-compliant autonomous Guidance, Navigation, and Control (GNC) scheme, and the monitoring agent prototype for actively ensuring fault tolerance. These innovations aim to enhance the safety, adaptability, and reliability of autonomous vessels operating across diverse European waterborne environments. It is of high importance to achieve this aim considering that autonomous navigation in inland waterways and short-sea operations face critical challenges: dynamic environments, differences in traffic rules between geographical areas of different jurisdiction, risks posed by abnormal events (e.g., faults) and mixed traffic scenarios involving both manned and autonomous traffic participants.

The deliverable demonstrates a significant step toward intelligent, rule-aware, and fault-resilient autonomous vessel navigation. It concerns the design of an intelligent GNC scheme, whose primary role is to dynamically (i) estimate the position and velocity of the vessel using sensors including GNSS, gyrocompass, Inertial Measurement Unit (IMU), Automatic Identification System (AIS), and perceive the operational environment (navigation), (ii) compute the path/trajectory that the vessel should follow (guidance), and (iii) render the vessel follow the computed path/trajectory (control).

Funded by the European Union

Funded by the European Union. Views and opinions expressed are however those of the author(s) only and do not necessarily reflect those of the European Union or CINEA. Neither the European Union nor CINEA can be held responsible for them. Grant Agreement N° 101096923.

The GNC scheme that we developed in Task 4.2 is also able to **(i)** handle the effects of malfunctions (fault-tolerance), and **(ii)** effectively switch between applicable regulations when the operational environment changes (i.e., when the vessel transits from inland waterways to a port area). “COLREG-compliance” is “achieved by exploring the capability to express regulations with a suitable mathematical representation and deriving requirements for sensors, including water depth sensors (e.g., sonars) or lidars/cameras to avoid collision with spatial boundaries (where the GNSS measurements are not accurate).”, using semantics and a modular Finite-State Machine in Chapter 2. More specifically, traffic regulations are transcribed as ontologies in a navigation-oriented database (.owl format). Safe distance requirements from other traffic participants and from spatial boundaries, and velocity requirements are translated as sensor requirements for the determination of the traffic roles (e.g., stand-on, give-way vessel) in Chapter 2, and for the determination of a safe trajectory deviation to avoid collisions in Chapter 4. To manage mixed traffic conditions, we establish a new traffic role for emergency situations where compliant actions are not applied. The novelty of embedding regional regulations (e.g., BPR) as part of the semantic database with the COLREGS and of the Finite-State Machine (Chapter 2) addresses the need to handle “the effect of COLREGs alterations on this predicament”. Fault-tolerance is “implemented through the development of a monitoring module capable of: (i) detecting local fault occurrence, (ii) isolating the fault type (e.g. sensor fault, engine fault) and/or location (e.g. radar sensor fault, GNSS sensor fault), (iii) distinguishing between local faults and falsified communicated data (e.g. spoofing of AIS data) and propagated faults”, with the relevant design showcased in Chapter 3. To handle the effects of “falsified communicated data”, the diagnosis logic design in Section 3.1 considers the propagation of sensor faulty information via the communication of monitoring agents and distinguishes between local and propagated sensor faults. The management of “remedial actions (e.g. by reconstructing the faulty sensor information using virtual sensors, or by using virtual actuators to reconstruct the actions, or by adapting the controller)” is handled by a high-level risk mitigation framework developed to interact with the GNC system in Chapter 4. As a result, the vessel operation can always result in a safe fallback state. The “fault-tolerant capabilities” of the GNC scheme are enhanced by embedding virtual sensors as part of the Guidance system in Chapter 4. Virtual sensors quantitatively express the “analytical redundancy” of the system and help reduce hardware “redundancy requirements” (i.e., duplicate sensors) onboard the vessel.

The methods presented in this work have the potential to work alongside and boost the performance of other important SEAMLESS solutions, such as the low-attention Remote Operation Center (ROC) architecture and ModalNET. The reasons for that are the collision-free and fault-tolerant capabilities, which would allow for higher system uptime, continuous support in the decision making by remote operators, and fewer disruptions in the waterway traffic network (i.e.., due to the avoidance of accidents). The proposed solutions contribute to the SEAMLESS vision of safe and autonomous waterborne transport.

Funded by the European Union

Funded by the European Union. Views and opinions expressed are however those of the author(s) only and do not necessarily reflect those of the European Union or CINEA. Neither the European Union nor CINEA can be held responsible for them. Grant Agreement N° 101096923.

TABLE OF CONTENTS

Funded by the European Union

Funded by the European Union. Views and opinions expressed are however those of the author(s) only and do not necessarily reflect those of the European Union or CINEA. Neither the European Union nor CINEA can be held responsible for them. Grant Agreement N° 101096923.

Funded by the European Union

Funded by the European Union. Views and opinions expressed are however those of the author(s) only and do not necessarily reflect those of the European Union or CINEA. Neither the European Union nor CINEA can be held responsible for them. Grant Agreement N° 101096923.

LIST OF FIGURES

Funded by the European Union

Funded by the European Union. Views and opinions expressed are however those of the author(s) only and do not necessarily reflect those of the European Union or CINEA. Neither the European Union nor CINEA can be held responsible for them. Grant Agreement N° 101096923.

LIST OF TABLES

Funded by the European Union

Funded by the European Union. Views and opinions expressed are however those of the author(s) only and do not necessarily reflect those of the European Union or CINEA. Neither the European Union nor CINEA can be held responsible for them. Grant Agreement N° 101096923.

LIST OF ABBREVIATIONS

Abbreviation	Description
3-D	3-Dimensional
ALOS	Adaptive LOS
ARR	Analytical Redundancy Relation
AI	Artificial Intelligence
ASV	Autonomous Surface Vessel
BBN	Bayesian Belief Network
BPR	Binnenvaartpolitiereglement
COLREGs	Convention on the International Regulations for Preventing Collisions at Sea
DoF	Degrees-of-Freedom
DNV	Det Norske Veritas
DUC	Demo Use Case
DVL	Doppler Velocity Log
EGW	Emergency GW (traffic role)
ELOS	Extended-state-observer-based LOS
FDI	Fault Detection, Isolation and Identification
FDIR	Fault Detection, Isolation, and Reconfiguration
FSM	Fault Signature Matrix
FTC	Fault-Tolerant Control
FPS	Feasible Parameter Set
GW	Give-way (traffic role)
GNC	Guidance, Navigation and Control
IMU	Inertial Measurement Unit
IWT	Inland Waterway Transport
ILOS	Integral LOS
LOS	Line-of-Sight
MRC	Minimum-Risk Condition
MCTS	Monte Carlo Tree Search
POMDP	Partially Observable Markov Decision Process
PRR	Police Regulations for the Navigation of the Rhine
PLOS	Proportional LOS
RIF	Risk-Influencing Factor
R&T	Rudders and Thruster
ROC	Remote Operation Center
SCS	Safe Control Strategy
SME	Set-Membership Estimation
SSS	Short-Sea Shipping
SOG	Speed Over Ground
SO	Stand On (traffic role)
STPA	Systems Theoretic Process Analysis
UPS	Unfalsified Parameter Set
UCB	Upper Confidence Bound
VO	Velocity Obstacle

Funded by the European Union

Funded by the European Union. Views and opinions expressed are however those of the author(s) only and do not necessarily reflect those of the European Union or CINEA. Neither the European Union nor CINEA can be held responsible for them. Grant Agreement N° 101096923.

Funded by the European Union

Funded by the European Union. Views and opinions expressed are however those of the author(s) only and do not necessarily reflect those of the European Union or CINEA. Neither the European Union nor CINEA can be held responsible for them. Grant Agreement N° 101096923.

1 INTRODUCTION

Nowadays, waterborne transport is responsible for more than 80 % of global cargo services (Pratson, 2023). To realise the European's Green Deal's target of climate-neutrality by 2050, the shift from road transport to inland waterways and the automation of multi-modal mobilities have been identified as two of the European Union's thematic priorities (Smeds & Cavoli, 2021). Effectively, pursuing those goals in the maritime domain would require **(1)** the seamless adaptation of marine vessels in multi-environment (e.g., Inland Waterways, Short-Sea) operations, and **(2)** the enhancement of the operational safety of new autonomous vessel concepts.

Motion planning and control are essential functionalities for navigation in diverse environments. These tasks are usually handled by a dedicated Guidance, Navigation and Control (GNC) system, such as the SEAMLESS proposed GNC system shown in Figure 1. **Guidance** is the function of an experienced helmsman (F. Liu et al., 2019), responsible for motion planning since it is used to assess the navigational situation and provide the reference signals to the controller (e.g., reference heading). The most safety-critical guidance objective is the planning of a safe path for the vessel to avoid collisions with other traffic participants, and the surrounding infrastructure. Processed sensor information is typically communicated to the Guidance from the Navigation system, during the vessel's operation. The **navigation** system integrates multiple hardware sensors to determine the vessel's position, velocity, and orientation. Like any hardware component, these sensors are susceptible to faults. Sensor faults problem is usually overlooked; however their effects may result in accidents such as collisions. Finally, the **control** system is responsible for the implementation of the guidance decisions, using the information from the navigation system. Path following, and collision avoidance are standard operational objectives handled by this system. Considering collision avoidance, the implemented system should be able to handle the vessel interactions with other traffic participants (i.e., manned or unmanned vessels) and the surrounding infrastructure (e.g., locks, bridges, banks).

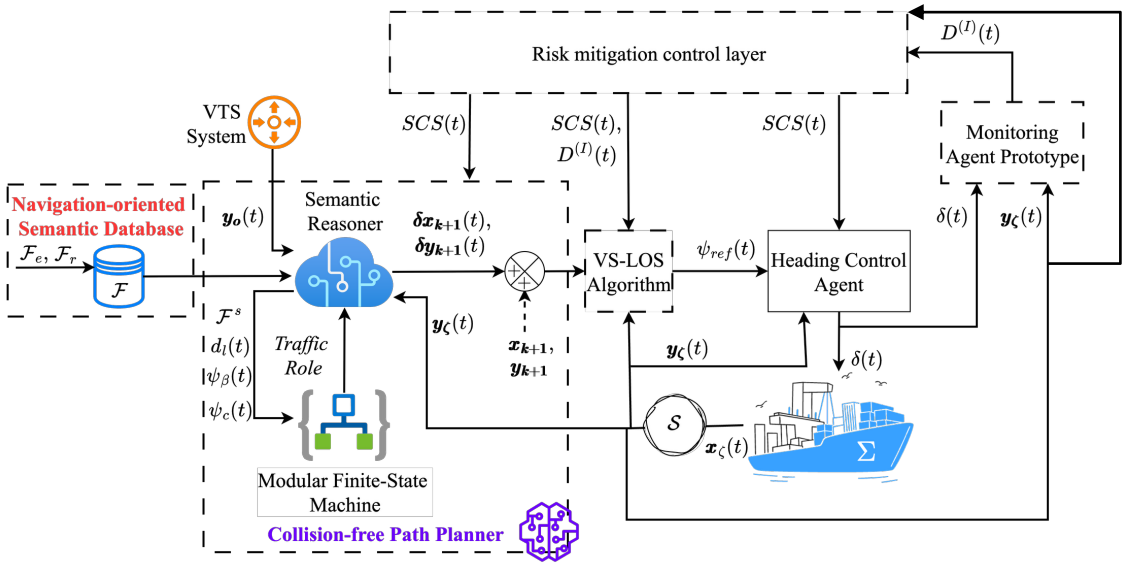

Figure 1 GNC scheme developed in Task 4.2 featuring fault-tolerant and collision-free guidance capabilities. The novelties presented in this report are shown with dashed boxes.

Funded by the European Union

Funded by the European Union. Views and opinions expressed are however those of the author(s) only and do not necessarily reflect those of the European Union or CINEA. Neither the European Union nor CINEA can be held responsible for them. Grant Agreement N° 101096923.

The operational environment is associated with different spatial constraints (e.g., water depth, port/ waterway topology) that influence the dynamic behaviour of the vessel (e.g., bank/squat effects). In addition, different applicable traffic rules determine the expected behaviour of the vessel (e.g., actions to avoid collision). Most of the available literature considers traffic rules expressed in the Convention on the International Regulations for Preventing Collisions at Sea, 1972, commonly referred to as COLREGs. Meanwhile, regional regulations applicable to Inland Waterway traffic, such as the Binnenvaartpolitiereglement (BPR) (Overheid.nl, 2025) and the Police Regulations for the Navigation of the Rhine (PRR) (Commission Centrale pour la Navigation du Rhin (CCNR), 2024) are not adequately discussed (Hu et al., 2022; Tran et al., 2023). When the vessel navigates in port areas and inland waterways of different flag states, the difference in the expected traffic behaviour should be recorded (e.g., using a semantic database like the one in Figure 1), and implemented by the collision avoidance system, to successfully prevent accidents and secure the infrastructure investments.

1.1 NAVIGATIONAL RISK MITIGATION

According to the European Maritime Safety Agency (European Maritime Safety Agency, 2025), over the period 2014-2024, accidents of navigational nature (i.e., collisions, contacts, and groundings/strandings) represented almost 46.2 % of all occurrences. Moreover, another 26.1% of all incidents were attributed to loss of directional (e.g., rudder) and propulsion power (e.g., propeller). System failures (e.g., due to sensor or actuator faults) are often a root cause for the occurrence of loss of control events. To contain all these risks and reduce the number of accidents, proper collision avoidance systems and monitoring agents should be developed.

Hazard identification and risk assessment analysis are essential steps to ensure their safe and reliable operation of autonomous vessels. The use of techniques such as systems theoretic process analysis (STPA) has been widely explored in the literature for safety assessment and verification (Wróbel et al., 2018). Additionally, providing the analysis results as inputs to the control system during system operation can further enhance the decision-making capabilities of autonomous vessels (Thieme et al., 2023). Arguably, one of the most critical decision-making tasks is to identify a hazardous situation and prevent an accident by bringing the system to a minimum-risk condition (MRC). According to (DNV GL, 2018), an MRC is defined as “a temporary as-safe-as-possible state that the vessel enters when it experiences situations which, if continued, involves operating outside the safe operating envelope”. These situations can arise from unsafe actions taken during vessel operation, originating from factors such as sensor faults, communication delays, or sudden change of operational conditions (e.g., traffic environment, traffic rules), and can potentially disrupt nominal operations. Enhancing the operational safety against physical threats in the navigational environment (e.g., other vessels, infrastructure) should be equally important to the diagnosis and handling of malfunctions (e.g., faults), affecting the single vessel operation.

Partially observable Markov decision processes (POMDPs), on the other hand, can directly model the effect of decisions taken on the system’s state by incorporating them as “actions” in their framework. Furthermore, unlike the static structure of Bayesian networks, POMDPs offer a dynamic modeling approach that enhances their ability to assess risks more effectively. However, this approach to risk modeling for Autonomous Surface Vessels (ASVs) remains unexplored in the literature, as the number of states and associated properties in a POMDP model can rapidly

Funded by the European Union

Funded by the European Union. Views and opinions expressed are however those of the author(s) only and do not necessarily reflect those of the European Union or CINEA. Neither the European Union nor CINEA can be held responsible for them. Grant Agreement N° 101096923.

proliferate. This could significantly increase the computational cost of real-time evaluation, which stands as a key consideration favouring the adoption of Bayesian networks (Rothmund, 2023). Furthermore, determining the transition probabilities for the POMDP model is also a challenge.

1.2 State of the Art in Safety in the GNC Scheme

Typically line-of-sight (LOS) laws are very popular for the design of the Guidance system, due to their low computational cost and simplicity (Gu et al., 2022). The primary objective of LOS methods is to adjust the vessel's heading angle to minimize the cross-tracking error, i.e., the lateral deviation from the desired path. Extensions of the basic proportional LOS (PLOS) guidance law include integral LOS (ILOS) (Chen et al., 2024) and extended-state-observer-based LOS (ELOS) (Wu et al., 2024) guidance methods for compensating unknown sideslip and ocean currents. Adaptive LOS (ALOS) guidance laws have also attracted particular attention, as they are able to estimate uncertain parameters such as sideslip angle or current effects in real time, thereby improving robustness without relying on costly sensors. To this end, parameters such as the lookahead distance are varied (C. Liu et al., 2018) while others such as the unknown drift angle are estimated (F. Liu et al., 2019). In (Fossen, 2023), the authors develop an ALOS guidance law, able to compensate for drift forces due to wind, waves, and ocean currents. The performance of the proposed method is shown to be comparable to that of ILOS Guidance law, which assumes a fixed sideslip angle, with less overshoot than ELOS, which can handle rapidly varying sideslip angles. A 3-Dimensional (3D) ALOS guidance law is derived by the authors in (Fossen & Aguiar, 2024), considering both heading and depth-changing maneuvers. A stability proof for the guidance law is provided, although only under healthy conditions for the actuators and sensors (i.e., in the absence of faults). (Su et al., 2021) develop a similar adaptive guidance law , also providing the stability analysis for the guidance system. However, this work only considers the kinematic model of the vessel excluding the dynamical aspects (forces and moments). On the contrary, a 3-Degrees-of-Freedom (DoF) dynamical model is used by (X. Liu & Zhang, 2024), and actuator faults are modelled as loss of efficiency. Sensor noise as well as the influence of sensor faults are not considered though in the aforementioned research works. The timely diagnosis and mitigation of the effects of this type of faults is particularly important for the overall safety of the vessel, expressed by its accurate motion planning and collision avoidance capabilities.

In (Yang et al., 2019), a cooperative collision avoidance mechanism is developed for a network of vessels. The reference trajectory modification for each vessel is selected by a set of possible routes with different characteristics (e.g., closest time of approach between vessels) through the application of a genetic algorithm. Nonetheless, only vessel-to-vessel collisions are considered in their study while the generation of the initial reference trajectory for each vessel is left out of discussion. The authors of (Hinostroza et al., 2021) consider the risk of collision with static obstacles and propose a guidance scheme for trajectory tracking and collision avoidance. To this end, the Line Of Sight (LOS) algorithm is used to calculate the reference heading based on the vessel's position and its reference trajectory. Collision avoidance is reinforced by selecting a deviation from the reference trajectory through an optimization process, similar to Dijikstra's algorithm, called the Fast Marching method. The use of LOS is discussed in (Li et al., 2023) considering collisions with both other vessels and static obstacles. Through the formulation of vessel speed and distance constraints in a robust optimisation framework, the optimal course deviation is selected and collisions are avoided. While

Funded by the European Union

Funded by the European Union. Views and opinions expressed are however those of the author(s) only and do not necessarily reflect those of the European Union or CINEA. Neither the European Union nor CINEA can be held responsible for them. Grant Agreement N° 101096923.

the previous papers contribute significantly to the minimization of the deviation from the original route to avoid collisions, the proposed algorithms are associated with high complexity and can prove computationally intensive in heavy traffic scenarios.

Considering traffic rule-awareness, ongoing research has mostly focused on incorporating COLREGs in the motion planning algorithm. In (Tsolakis, et al., 2024), the authors address the problem of determining the traffic scenario and decision-making using the dynamically computed relative bearing and heading between the vessels and a Finite-State Machine Approach. The integration of the guidance subsystem in the controller, through rule-compliant constraint generation, significantly streamlines the implementation at the expense of modularity in the GNC scheme. (Hinostroza et al., 2021) discuss a combination of the LOS algorithm for trajectory tracking with the Velocity Obstacle (VO) method for collision avoidance. VO optimises the generated trajectory deviation based on information about the own vessel's course and position, the other vessel's position, velocities and the safe distance between vessels. The computational burden associated with the optimisation process is addressed by a pseudo-algorithm, though the implementation aspects of obtaining and using the information about other vessels and obstacles are left out of the discussion. (He et al., 2022; Zhao et al., 2022) also employ the VO method for collision avoidance, further integrating COLREGS, while (Zhou et al., 2022) propose stream functions to calculate the course deviation for collision avoidance, inspired by the field of hydrodynamics. Nevertheless, the previous methods consider that both the position and the velocities of other vessels are known, excluding details on how this information is obtained. Regarding learning-based methods, Deep Reinforcement learning algorithms for vessel-to-vessel collision avoidance are investigated in single and cooperative AI agent settings in (Yoshioka et al., 2024; Yoshioka & Hashimoto, 2022). Positive and negative rewards are assigned when the vessel follows the waypoints, enters defined dangerous areas for collision, and performs according to the traffic rules. The assignment of the traffic roles to the involved vessels is left out of the discussion, though.

1.3 State of the Art in Monitoring Capabilities of GNC Scheme

To enable safe autonomous vessel operations, multiple sensors and actuators must be installed and integrated before the intended operation in the Navigation system of the GNC scheme. These hardware components are susceptible to faults, due to exposure in the harsh marine environment, wear and degradation. One or multiple monitoring agents are designed to handle the tasks of Fault Detection, Isolation and Identification (FDI), enabling the system to precisely pinpoint and identify the nature, location and magnitude of the fault. The design of the agents should also be incorporated in the safety design philosophy, as part of the GNC scheme.

Considering sensor faults, (Q. Zhang et al., 2021) proposed a nonlinear observer for sensor fault estimation, which is subsequently employed in designing a fault-tolerant model reference reinforcement learning control scheme to guarantee stable tracking for ASVs. The proposed scheme assumes the occurrence of a single fault, limiting its capability of isolating multiple sensor faults. In the work of (Blanke, 2006), structural analysis is performed to exploit the analytical redundancy of sensors for fault diagnosis, accompanied by a fault-tolerant fusion of sensor data. In (Rogne et al., 2014) the authors proposed a scheme for the FDI of navigational sensors using a nonlinear observer in conjunction with a “reliable” inertial measurement unit (IMU) sensor. A limitation of the model-based schemes proposed in (Blanke, 2006; Rogne et al., 2014) is that the effects of modelling

Funded by the European Union

Funded by the European Union. Views and opinions expressed are however those of the author(s) only and do not necessarily reflect those of the European Union or CINEA. Neither the European Union nor CINEA can be held responsible for them. Grant Agreement N° 101096923.

uncertainties such as external disturbances (e.g. wind force) on vessel kinetics are not considered. Wind forces represent the dominant external force in ports and inland waterways (Kepaptsoglou et al., 2015) and may lead to erroneous fault diagnosis if neglected.

In case of faults affecting the on-board sensors, additional hardware redundancy in the design has been proposed so far as a way to recover operation. Alternatively, the automation design could benefit from the availability of heterogeneous sensors and model information to construct virtual (software-based) sensor instances. The concept of virtual sensors remains underexplored in maritime applications, with only a limited number of studies addressing the topic (Bryne et al., 2017; Hashemi & Shami, 2021). These cyber devices offer several advantages, including lower installation costs and the lack of spatial constraints. When sensors are affected by faults, the vessel's safety and control stability can be ensured by switching between hardware and virtual sensors.

Regarding the monitoring of actuator faults, in (Corradini et al., 2011), an actuator fault-tolerant control scheme designed for an underwater Remotely Operated Vehicle integrates detection, isolation, and accommodation modules. This work relies on residual generation modules for detection and exploits the specific actuator configuration for isolation through the sliding surface of a designed sliding mode controller (Cocquempot et al., 1998). The same vehicle was studied in (Freddi et al., 2013) where the authors focus on the problem of detection only, based on a nonlinear Thau observer for residual generation and on a sequential change detection algorithm for residual evaluation. In (Baldini et al., 2022a), an active Fault Diagnosis method is proposed for the same system so that actuator faults can be discerned from other disturbances by applying an auxiliary sinusoidal input system that is designed to propagate into the control system when a fault occurs while having minimal impact on the system dynamics. In (Baldini et al., 2022b), a bank of observers is used for FDI in cascade with a nonlinear disturbance observer for fault estimation under the assumption that only a single fault may occur. Fault detection, which is only the first step of fault diagnosis, was studied for an underactuated surface vessel in (Park & Yoo, 2016), where a robust fault detection observer and a time-varying detection criterion are presented to detect the actuator faults distinguished from uncertainties and external disturbances. A Fault-Tolerant Control (FTC) strategy for linear systems is proposed in (Cristofaro & Johansen, 2014) with active FD that relies on the control redundancy of an overactuated ASV by constraining the inputs in prescribed configurations for Fault Detection, Isolation, and Reconfiguration (FDIR). However, this work relied on the linearization of vessel dynamics, assuming that the vessel’s rotation is negligible.

1.4 Structure of the Document

This document is structured in 6 chapters.

Chapter 2 focuses on the integration of traffic rules in the GNC scheme, to allow the seamless adaptation of ASVs to both Short-sea and Inland waterway operations;

Chapter 3 focuses on the design of the monitoring architecture, built to handle both sensor and actuator faults;

Funded by the European Union

Funded by the European Union. Views and opinions expressed are however those of the author(s) only and do not necessarily reflect those of the European Union or CINEA. Neither the European Union nor CINEA can be held responsible for them. Grant Agreement N° 101096923.

Chapter 4 discusses the specifics of the developed GNC scheme, including the management of remedial actions, fault-tolerant and collision-free path planning and the integration of semantic reasoning;

Chapter 5 provides application results for the proposed methods, using multiple Use Cases. The Use Cases are linked to the Task 4.2 Description in the Grant Agreement.

Chapter 6 concludes the document, summarizing the findings and linking to SEAMLESS defined Key Performance Indicators (KPIs).

2 INTEGRATION OF TRAFFIC RULES IN THE GNC SCHEME

The integration of traffic rules in the GNC scheme is done considering two aspects; (1) the GNC system should be aware of the rule-context and the characteristics of the operational environment, and (2) the matching between the encounter situations (e.g., head-on) and the traffic roles (e.g., stand on) should be clearly defined. The first task is handled using semantic annotation tools and is presented in Section 2.1. A modular Finite-state Machine Approach is used to handle the second task, with the relevant design presented in Section 2.2. **This research is featured as part of the SEAMLESS registered publication (Kougiatsos et al., 2026).** It is worth to note that the integration of traffic rules is necessary for mixed traffic environments, assuming that the manned vessels will follow the rules. When there is unexpected deviation from the rules, the proposed GNC scheme takes emergency actions to preserve safety.

2.1 TRANSLATION OF TRAFFIC RULES IN ONTOLOGIES

A semantic database $\mathcal{F}$ can be defined for navigational purposes as (Kougiatsos et al., 2026):

$$\mathcal{F} = \mathcal{F}_e \cup \mathcal{F}_r, \tag{1}$$

where $\mathcal{F}_e$ stores the semantic information on the vessel's "operational environment" and $\mathcal{F}_r$ stores the semantic information related to the "traffic rules" that the vessel should follow. These concepts are further outlined as follows:

- ``**Operational environment**'': During the vessel's mission, the type of operational environment dictates the physical infrastructure limitations that the vessel is required to consider (e.g., waterway width and water depth).
- ``**Traffic Rules**'': Depending on the location where the vessel operates, certain rules will dictate its traffic behaviour. These rules can be generally categorized in **three categories**, the ``**Situation Invariant Rules**'', ``**Situation Analysis Rules**'' and ``**Situation Dependent Rules**''. The first are always followed regardless of the traffic scenario. A vessel can assume one of the following three roles in an encounter situation with another vessel; Stand On (when expected to keep the same course and speed), Give-way (when expected to take collision avoidance action) and Emergency Give-way (in situations when the Stand-On vessel finds herself so close to collision and is expected to take any action to aid in avoiding said collision). ``Situation Analysis Rules`` are used to assign the role (i.e., give-way, stand-on and emergency give-way) of the vessel in the specific encounter scenario. ``Situation Dependent

Funded by the European Union

Funded by the European Union. Views and opinions expressed are however those of the author(s) only and do not necessarily reflect those of the European Union or CINEA. Neither the European Union nor CINEA can be held responsible for them. Grant Agreement N° 101096923.

Rules`` are used to dictate a safe distance from other vessels, a safe lane distance and a safe speed for the own vessel, depending on the traffic role and encounter situation.

To realise the semantic database, the open-source software Protégé is used, as shown in Figure 2. Classes are created for traffic rules ($\mathcal{F}_r$), the operational environment ($\mathcal{F}_e$), while future expansions might include the “sensors”, multiple types of “vessels”, the vessel “design space”, “operator profiles” etc. Two additional classes, namely “encounter situations” and “operational actions” are used to interface with the methods in Section 2.2 and Chapter 3, respectively. The result of the software is a Web Ontology Language (OWL) document, which can be later be accessed by the GNC scheme.

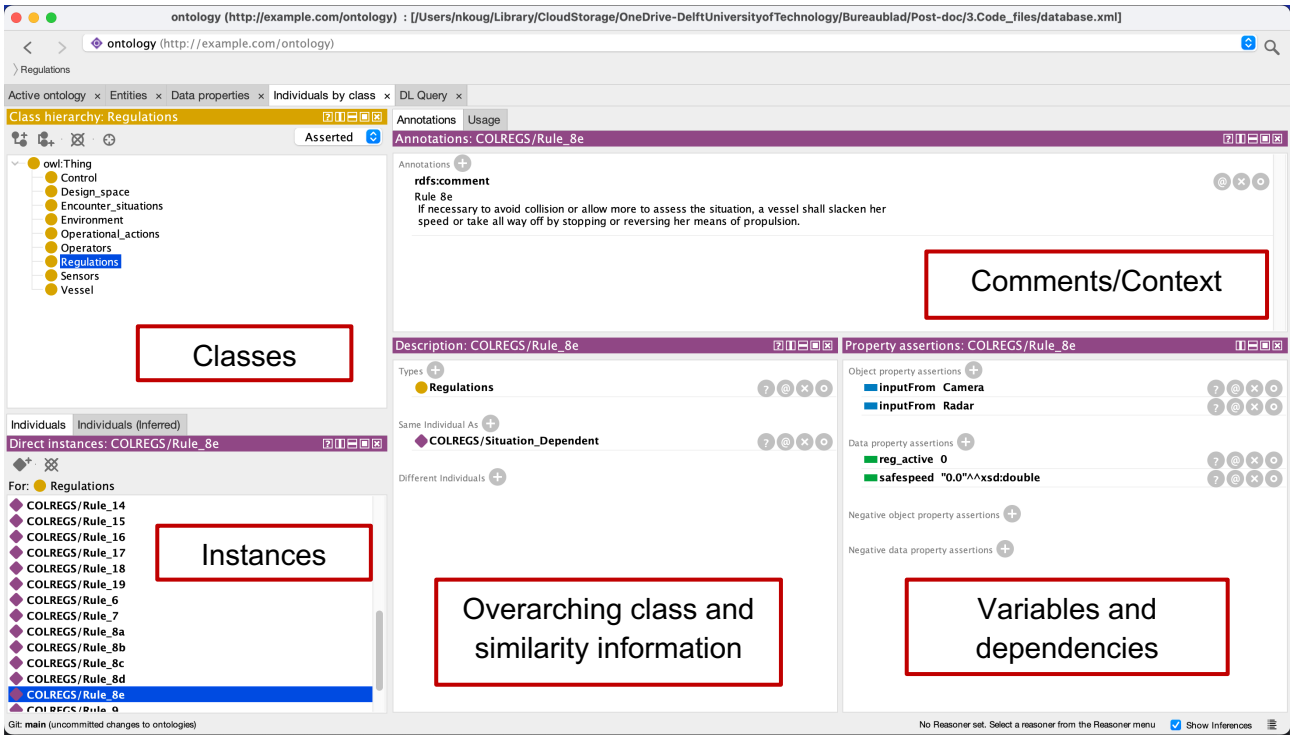

Figure 2 Semantic Translation of traffic rule requirements using Protégé

2.2 Modular Finite-State Machine

In open and short-sea environments, where COLREGs are in effect, the traffic roles can be related to specific encounter situations, as (Tsolakis, Negenborn, et al., 2024):

- **Give way (GW):** Head-On, Overtaking and Starboard-Crossing
- **Stand-On (SO):** Port-Crossing and Overtaken with no needed action
- **Emergency give way (EGW):** Port-Crossing and Overtaken with emergency action

For inland waterway navigation, different traffic rules apply (i.e., BPR, PRR) and the relation between the traffic roles and encounter situations can changes. For instance, according to Chapter 6 of BPR (Overheid.nl, 2025), the following different-to-COLREGS traffic rules apply (Kougiatsos et al., 2026):

- **Head-on situation (Article 6.04):** If two vessels are approaching each other on opposite courses in such a way that there is a risk of collision, the vessel not following the starboard

Funded by the European Union

Funded by the European Union. Views and opinions expressed are however those of the author(s) only and do not necessarily reflect those of the European Union or CINEA. Neither the European Union nor CINEA can be held responsible for them. Grant Agreement N° 101096923.

side of the fairway shall give-way to the vessel following the starboard side of the fairway. If neither vessel follows the starboard side of the fairway, each shall give-way to vessels on the starboard side so that they pass each other port to port.

- **Crossing situation (Article 6.17):** If the courses of two ships cross each other in such a way that there is a risk of collision, the vessel not following the starboard side of the fairway shall give way to the vessel following the starboard side of the fairway. In case none of the ships follows the starboard side of the fairway, the ship approaching from the port side gives way to the vessel approaching from starboard side.

Thus, the relation of the traffic role and the various encounter situations changes to (Kougiatsos et al., 2026):

- **GW:** Head-On (port side of the waterway), Overtaking and Crossing (port side of the waterway),
- **SO:** Head-On (starboard side of the waterway),Crossing (starboard side of the waterway) and Overtaken with no needed action,
- **EGW:** Crossing (starboard side of the waterway) and Overtaken with emergency action,

with the lane distance from the port and starboard side of the waterway, the relative heading and the relative bearing between the vessels being important parameters for the role assignment.

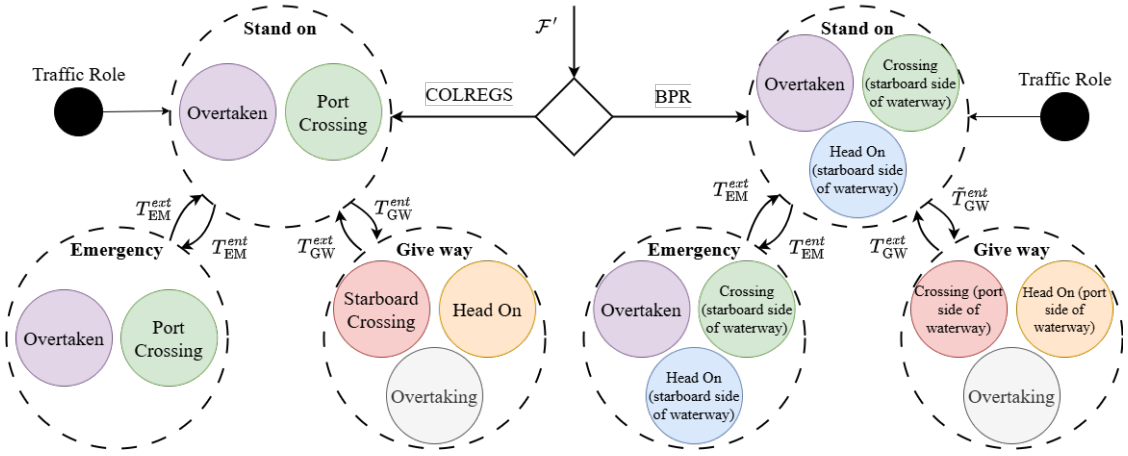

Figure 3 Assignment of the Traffic Role using a modular Finite-state Machine Approach.

The traffic role of the own vessel and other vessels can be determined using a Finite-State Machine approach, as shown in Figure 3. When COLREGS are in effect, the design of the left-hand side Finite-State Machine in Figure 3 has been already described in (Tsolakis, Negenborn, et al., 2024). Following a similar rationale, we construct the Finite-State Machine corresponding to BPR traffic rules and shown in the right-hand side of Figure 3.

The following conditions are used for the determination of the traffic role of the own and other vessels during an encounter. In the case of COLREGs, the conditions have been adequately defined in (Tsolakis, Negenborn, et al., 2024), whereas in (Kougiatsos et al., 2026), the authors of this deliverable derived the conditions for BPR. As a result, the Finite-State Machine in Figure 3 is composed by two branches.

Funded by the European Union

Funded by the European Union. Views and opinions expressed are however those of the author(s) only and do not necessarily reflect those of the European Union or CINEA. Neither the European Union nor CINEA can be held responsible for them. Grant Agreement N° 101096923.

- COLREGs Branch:
  See (Tsolakis, Negenborn, et al., 2024)

- BPR Branch:
  As featured in (Kougiatsos et al., 2026), the following conditions apply:

$$\tilde{T}_{ent}^{GW} = T_{enc} \wedge \left\{ T_{rsk} \wedge \left[\left((T_{hdn} \vee T_{str}) \wedge T_{bpr} \wedge \neg T_{stb} \right) \vee \left(T_{brn} \wedge (T_{ovr} \vee T_{stb}) \right) \right] \right\}, \quad (2)$$

$$T_{GW}^{ext} = \neg T_{enc}, \quad (3)$$

$$T_{EM}^{ent} = T_{emg}, \quad (4)$$

$$T_{EM}^{ext} = \neg T_{emg}, \quad (5)$$

where the logic symbols ∧,∨, ¬ stand for “and”, “or” and “not” respectively,

$$T_{enc} = d(t) < \rho_{enc}, \quad (6)$$

$$T_{rsk} = d_{CPA}(t) < \rho_p + \rho_q + \rho_s, \quad (7)$$

$$T_{hdn} = (\psi_c(t) \geq \pi - \psi_h) \wedge (\psi_c(t) < \pi + \psi_h), \quad (8)$$

$$T_{str} = (\psi_c(t) \geq \pi + \psi_h) \wedge \left(\psi_c(t) < \frac{13\pi}{8}\right), \quad (9)$$

$$T_{brn} = \left(\psi_c(t) \geq \frac{13\pi}{8}\right) \wedge \left(\psi_c(t) < \frac{3\pi}{8}\right), \quad (10)$$

$$T_{ovr} = \left(\pi + \psi_\beta(t) - \psi_c(t) \geq \frac{5\pi}{8}\right) \wedge \left(\pi + \psi_\beta(t) - \psi_c(t) < \frac{11\pi}{8}\right), \quad (11)$$

$$T_{stb} = \left(\psi_\beta(t) \geq 0\right) \wedge \left(\psi_\beta(t) < \frac{5\pi}{8}\right), \quad (12)$$

$$T_{emg} = d(t) < \rho_{emg}, \quad (13)$$

with $\psi_h \cong 6\,deg$, and ρ_{emg} defining the radius of a circular area around the ASV within which, if a GW vessel enters, it is inferred it does not comply with the rules. The evaluation of conditions (2)-(13) for BPR and the corresponding conditions for COLREGs (Tsolakis, Negenborn, et al., 2024) requires input from sensors of the navigation system, as recorded in the following Table 1.

To evaluate the transition conditions and define the traffic role, the “sensor requirements” (as mentioned in the Task 4.2 description) are summarized in Table 1.

Table 1 Sensor requirements for the evaluation of conditions (2)-(13).

Sensor	Measured Parameter(s)	Useful for parameter calculation	Input to condition
GNSS	Position (latitude, longitude)	Distance between vessels d, Closest point of approach distance d_{CPA}, Relative bearing ψ_β	(6), (7), (11)-(13)
Dual-Antenna GNSS or Gyrocompass or Magnetic Compass	Heading	Relative heading ψ_c, Relative bearing ψ_β	(8)-(12)

Funded by the European Union

Funded by the European Union. Views and opinions expressed are however those of the author(s) only and do not necessarily reflect those of the European Union or CINEA. Neither the European Union nor CINEA can be held responsible for them. Grant Agreement N° 101096923.

Doppler Velocity Log	Velocity through water or over ground in surge, sway directions	Closest point of approach distance d_{CPA}	(7)
AIS (Automatic Identification System)	Other vessel's position (latitude, longitude), heading, and speed	Distance between vessels d, Closest point of approach distance d_{CPA}, Relative bearing ψ_β, Relative heading ψ_c	(6)-(13)

3 MONITORING AGENT PROTOTYPE

This Chapter presents the design of the monitoring agent prototype. This agent is responsible for the timely diagnosis of both sensor and actuator faults affecting the vessel navigation. Multiple monitoring agents are designed for the diagnosis of faults affecting the navigation sensors, while a single agent handles the diagnosis of actuator faults, as shown in Figures 4a and 4b, respectively. **The presented research are featured in the SEAMLESS registered publications (Dhyani, et al., 2024a; Tsolakis, et al., 2024a, 2024b).**

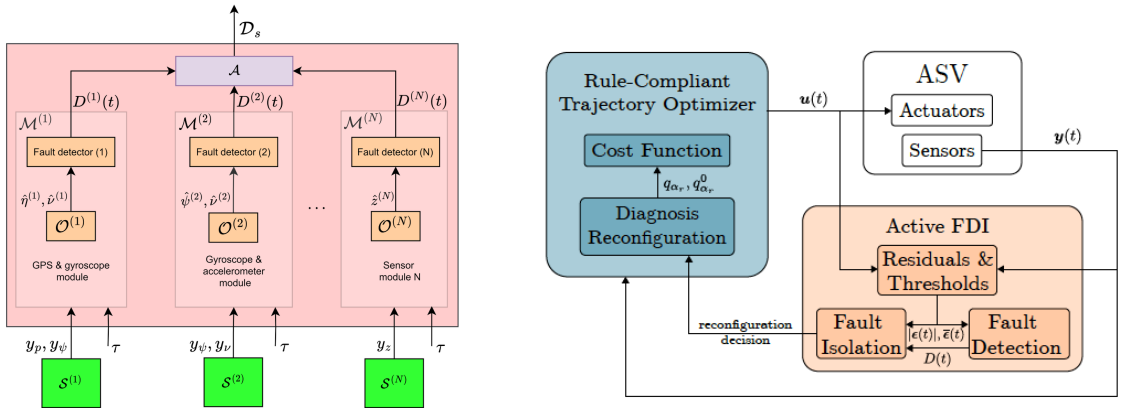

(a) **(b)**

Figure 4 Developed fault diagnosis frameworks considering (a) sensor (Dhyani, et al., 2024a) and (b) actuator faults (Tsolakis, et al., 2024a).

3.1 DIAGNOSIS OF SENSOR FAULTS

The material of this section is featured in the SEAMLESS registered publication (Dhyani et al., 2024). Sensor fault diagnosis, as shown in Figure 6a, is performed by a bank of monitoring modules, designed to have structured sensitivity to a set of sensor faults, i.e. Module $M^{(I)}$ is sensitive and detects faults in the set of sensors $S^{(I)}$. The decision on the detection of a fault is obtained based on a set of Analytical Redundancy Relations (ARRs) of residuals $\epsilon_{y_\zeta}^{(I,j)}$ and adaptive thresholds $\bar{\epsilon}_{y_\zeta}^{(I,j)}$ (the computation of residuals and adaptive thresholds is presented in the next section). For the monitoring module $M^{(I)}$, the set of ARRs $\mathcal{E}_{y_\zeta}^{(I)}$ are defined for detecting faults in the sensor set $S^{(I)}$,

Funded by the European Union

Funded by the European Union. Views and opinions expressed are however those of the author(s) only and do not necessarily reflect those of the European Union or CINEA. Neither the European Union nor CINEA can be held responsible for them. Grant Agreement N° 101096923.

as $\mathcal{E}_{y_\zeta}^{(I)} = \cup_j \left(\mathcal{E}_{y_\zeta}^{(I,j)}\right)$. If for example $I \in \{1,2\}$, then the $j-$th ARR $\mathcal{E}_{y_\zeta}^{(I,j)}$ is given by (Dhyani et al., 2024):

$$\mathcal{E}_{y_\zeta}^{(1,j)}: \left|\epsilon_{y_\zeta}^{(1,j)}\right| - \bar{\epsilon}_{y_\zeta}^{(1,j)} \leq 0, j \in \{1,2,3\}, \tag{14}$$

$$\mathcal{E}_{y_\zeta}^{(2,j)}: \left|\epsilon_{y_\zeta}^{(2,j)}\right| - \bar{\epsilon}_{y_\zeta}^{(2,j)} \leq 0, j \in \{1,2,3,4\}. \tag{15}$$

A violation of the $j-$th ARR implies the occurrence of at least one sensor fault in the corresponding sensor set $S^{(I)}$. Let define $T_D^{(I,j)}$ to be the first instance of violation of the $j-$th ARR $\mathcal{E}_{y_\zeta}^{(I,j)}$ in $M^{(I)}$, i.e., (Dhyani et al., 2024):

$$T_D^{(I,j)} = \min\left\{t: \left|\epsilon_{y_\zeta}^{(I,j)}\right| - \bar{\epsilon}_{y_\zeta}^{(I,j)} > 0\right\}. \tag{16}$$

The **fault detection** time for module $M^{(I)}$ is defined as $T_{FD}^{(I)} = \min_t \left\{T_D^{(I,j)}, \forall j\right\}$. The output of the monitoring module $M^{(I)}$ is the $I-$th decision $D^{(I)}(t) = \left[D^{(I,1)}(t), \ldots, D^{(I,m_I)}(t)\right]^\top$, where (Dhyani et al., 2024),

$$D^{(I,j)}(t) = \begin{cases} 0, if\ t < T_D^{(I,j)} \\ 1, if\ t \geq T_D^{(I,j)} \end{cases}. \tag{17}$$

3.1.1 Residual generation and adaptive threshold formulation

Let us consider $I = 1,2$. The residual vectors $\varepsilon_{y_\zeta}^{(I)} \in \mathbb{R}^{N_I}, I = 1,2$ are defined as the difference between the measurement of a state of the vessel (e.g. position) and its observer-based estimation (Dhyani, et al., 2024a)

$$\epsilon_{y_\zeta}^{(1)} = \begin{bmatrix} \epsilon_{y_\zeta}^{(1,1)} \\ \epsilon_{y_\zeta}^{(1,2)} \\ \epsilon_{y_\zeta}^{(1,3)} \end{bmatrix} = \begin{bmatrix} y_x \\ y_y \\ y_\psi \end{bmatrix} - \hat{\eta}^{(1)}, \tag{18}$$

$$\epsilon_{y_\zeta}^{(2)} = \begin{bmatrix} \epsilon_{y_\zeta}^{(2,1)} \\ \epsilon_{y_\zeta}^{(2,2)} \\ \epsilon_{y_\zeta}^{(2,3)} \\ \epsilon_{y_\zeta}^{(2,4)} \end{bmatrix} = \begin{bmatrix} y_\psi \\ y_u \\ y_v \\ y_r \end{bmatrix} - \begin{bmatrix} \hat{\psi}^{(2)} \\ \hat{\nu}^{(2)} \end{bmatrix}. \tag{19}$$

where $\hat{\eta}^{(1)} = \left[\hat{x}^{(1)}, \hat{y}^{(1)}, \hat{\psi}^{(1)}\right]$ is the estimation of the generalised position and heading vector $\eta = [x, y, \psi]^\top$, $\hat{\psi}^{(2)}$is the estimation of the heading and $\hat{\nu}^{(2)} = \left[\hat{u}^{(2)}, \hat{v}^{(2)}, \hat{r}^{(2)}\right]$ is the estimation of the generalized velocity vector $\nu = [u, v, r]^\top$. The estimation of these variables is derived using nonlinear observers designed based on the kinematic and kinetic model of the vessel. Particularly,

Funded by the European Union

Funded by the European Union. Views and opinions expressed are however those of the author(s) only and do not necessarily reflect those of the European Union or CINEA. Neither the European Union nor CINEA can be held responsible for them. Grant Agreement N° 101096923.

for $M^{(1)}$, being the monitoring module for the Galileo/GNSS and gyroscope sensors, the observer dynamics are described by (Dhyani et al., 2024)

$$\mathcal{O}^{(1)}:\begin{cases}\dot{\hat{\eta}} = R\left(\hat{\psi}^{(1)}\right)\hat{v}^{(1)} + K^{(1)}\tilde{\eta}^{(1)}, \\ \dot{\hat{v}}^{(1)} = M^{-1}\left(-C\left(\hat{v}^{(1)}\right)\hat{v}^{(1)} - D\left(\hat{v}^{(1)}\right)\hat{v}^{(1)} + \tau\right) + K^{(2)}R^{T}\left(\hat{\psi}^{(1)}\right)\tilde{\eta}^{(1)},\end{cases} \tag{20}$$

For $M^{(2)}$, being the monitoring module for the gyroscope and accelerometer sensors, the observer dynamics are described by (Dhyani, et al., 2024):

$$\mathcal{O}^{(2)}:\begin{cases}\dot{\hat{\psi}}^{(2)} = \hat{r}^{(2)} + K^{(3)}\,\tilde{\psi}^{(2)}, \\ \dot{\hat{v}}^{(1)} = M^{-1}\left(-C\left(\hat{v}^{(2)}\right)\hat{v}^{(2)} - D\left(\hat{v}^{(2)}\right)\hat{v}^{(2)} + \tau\right) + K^{(4)}\tilde{v}^{(2)},\end{cases} \tag{21}$$

where $\tilde{\psi}^{(2)} = y_{\zeta,3} - \hat{\psi}^{(2)}$ and $\tilde{v}^{(2)} = \left[y_{\zeta,4}, y_{\zeta,5}, y_{\zeta,6}\right]^{\top} - \hat{v}^{(2)}$. Here, $K^{(3)} \in \mathbb{R}$ and $K^{(4)} \in \mathbb{R}^{3\times3}$ is a diagonal matrix.

Under healthy sensor conditions (i.e., no sensor faults) the residuals should be bounded by certain thresholds that are necessary to capture the effects of unknown but bounded uncertainties (e.g. sensor noise). More specifically, the designed thresholds are adaptive and defined as (Dhyani, et al., 2024a):

$$\bar{\epsilon}_{y_\zeta}^{(1,j)} = E^{(1,j)} + \rho^{(1,j)}\Lambda_1^{(j)}\int_0^t Z^{(1,j)}(t)e^{-\xi^{(1,j)}(t-\tau)}dt + \bar{d}_j\,, for j \in \{1,2,3\}, \tag{22}$$

$$\bar{\epsilon}_{y_\zeta}^{(2,j)} = E^{(2,j)} + \rho^{(2,j)}\Lambda_2^{(j)}\int_0^t Z^{(2,j)}(t)e^{-\xi^{(2,j)}(t-\tau)}dt + \bar{d}_{j+2}\,, for j \in \{1,2,3,4\}, \tag{23}$$

where

$$E^{(1,j)}(t) = \rho^{(1,j)}e^{-\xi^{(1,j)}t}\bar{z}^{(1)} + \frac{\rho_d^{(1,j)}\,\bar{d}_j}{\xi_d^{(1,j)}}\left(1 - e^{-\xi_d^{(1,j)}t}\right) + \int_0^t \rho^{(1,j)}e^{-\xi^{(1,j)}(t-\tau)}\left[\bar{\tau}_e + \overline{\tilde{n}_\eta} + \begin{matrix}0\\(\tilde{\eta} - \tilde{v})\end{matrix}\right]dt, \tag{24}$$

$$E^{(2,j)}(t) = \rho^{(2,j)}e^{-\xi^{(2,j)}t}\bar{z}^{(2)} + \frac{\rho_d^{(2,j)}\,\bar{d}_{j+2}}{\xi_d^{(2,j)}}\left(1 - e^{-\xi_d^{(2,j)}t}\right) + \int_0^t \rho^{(2,,j)}e^{-\xi^{(2,j)}(t-\tau)}\begin{bmatrix}0\\ \bar{\tau}_e\end{bmatrix}dt, \tag{25}$$

$$Z^{(1,j)} = E^{(1,j)}(t) + \rho^{(1,j)}\Lambda_1^{(j)}\int_0^t E^{(1,j)}(t)e^{\left(\rho^{(1,j)}\Lambda_1^{(j)} - \xi^{(1,j)}\right)(t-\tau)}dt\,, \tag{26}$$

$$Z^{(2,j)} = E^{(2,j)}(t) + \rho^{(2,j)}\Lambda_2^{(j)}\int_0^t E^{(2,j)}(t)e^{\left(\rho^{(2,,j)}\Lambda_2^{(j)} - \xi^{(2,j)}\right)(t-\tau)}dt\,, \tag{27}$$

where $\rho^{(I,j)}, \xi^{(I,j)}, \rho_d^{(I,j)}, \xi_d^{(I,j)}$ are positive design constants satisfying $\left|e^{-K^{(I,j)}t}\right| \le \rho^{(I,j)}e^{-\xi^{(I,j)}t}$, $\xi^{(I,j)} > \Lambda_I^{(j)}\rho^{(1,j)}$, and $\Lambda_I^{(j)}$ are Lipschitz constants (i.e., represent the continuity of the system model equations), $K^{(I,j)}$ represent the elements of the gain matrices $K^{(I)}$, $(I,j) \in \{(1,1),(1,2),(1,3),(2,1),(2,2),(2,3),(2,4)\}$. The term $\bar{d}$ denotes the bound of the sensor noise.

Funded by the European Union

Funded by the European Union. Views and opinions expressed are however those of the author(s) only and do not necessarily reflect those of the European Union or CINEA. Neither the European Union nor CINEA can be held responsible for them. Grant Agreement N° 101096923.

3.1.2 Fault Isolation

Upon obtaining the decisions $D^{(I)}(t)$ from each monitoring module, **fault isolation** is performed by combining the decisions in the aggregator module A into a decision vector $D(t)$. Thereafter, a consistency test is performed between $D(t)$ and a binary fault signature matrix (FSM) F that consists of l rows, $l = \sum_I m_I$, with each row corresponding to the j−th ARR $\mathcal{E}_{y_\zeta}^{(I,j)}$, and $Nc = 2^s - 1$ columns, where s is the total number of monitored sensors. The q−th column F_q, $q \in \{1, \dots, Nc\}$ is referred to as a theoretical sensor fault pattern, and $F_{pq} = 1$ $(p \in \{1, \dots, l\})$, suggests that at least one sensor fault included in the combination F_{cq} is responsible for the violation of the ARR $\mathcal{E}_{y_\zeta}^{(I,j)}$, and therefore, affects $S^{(I)}$. $F_{pq} =$ " $*$ " is used instead of "1" to distinguish a possible violation due to the weak sensitivity of the ARR $\mathcal{E}_{y_\zeta}^{(I,j)}$ to a sensor fault included in F_{cq}. Otherwise, F_{pq} is taken to be zero. The observed fault pattern in $D(t)$ is said to be consistent with the theoretical pattern in F_q when $D_p(t) = F_{pq}, \forall p \in \{1, \dots, l\}$. Finally, the diagnosis set $D_s(t)$ is obtained as the output of the aggregator, which consists of all the possible fault combinations F_{cq}, obtained because of the consistency test. An example of an FSM is shown as Table 2 in Section 5.2.

3.2 Diagnosis of Actuator Faults

For the diagnosis of actuator faults (i.e. faults in the thrusters), as shown in Figure 4(b) a model-based approach, using observer-based residuals and adaptive thresholds, was developed (Tsolakis, et al., 2024a). However, considering that the actuator faults appear as variations of model parameters, a parameter identification technique was also developed following a Set-Membership Estimation (SME) approach. **This technique is analyzed in detail in the SEAMLESS registered publication (Tsolakis, et al., 2024b), and presented, as is, in this section.**

SME eliminates the need for knowing statistical distributions by relying solely on boundedness assumptions (Tsolakis, et al., 2024b). Fault Diagnosis based on SME facilitates a direct approach by concentrating on fault parameters rather than indirectly inferred residuals, employing inverse tests for fault detection, and concurrently estimating the feasible parameter set from historical input-output data (Tsolakis, et al., 2024b). The four steps of SME are shown in Figure 5, with more details on the first three and the last step provided in the follow-up subsections. The final subsection concerns the use of SME for fault diagnosis.

3.2.1 Set Membership Identification

This section explains the method to compute the Unfalsified Parameter Set (UPS) and the Feasible Parameter Set (FPS), within which the true faulty parameter lies. Supposing that the disturbance and noise are upper and lower bounded by $\bar{w}$, $\bar{d}$ respectively (i.e., $|w| \leq \bar{w}$, $|d| \leq \bar{d}$), the UPS can be derived as (Tsolakis, et al., 2024b):

$$\Delta_k = \left\{\theta \in \mathbb{R}^p \middle| -HG(u_{k-1})\theta \leq h_w + h_d + h_f(y_{k-1}) - Hy_k\right\}, \tag{28}$$

which can be computed at each time step k based on the input-output measurement set $\{u_{k-1}, y_{k-1}, y_k\}$. Term $h_d(\bar{d})$ directly sums the measurement bounds while $h_f\,(y_{k-1}, \bar{d})$ is a time-

Funded by the European Union

Funded by the European Union. Views and opinions expressed are however those of the author(s) only and do not necessarily reflect those of the European Union or CINEA. Neither the European Union nor CINEA can be held responsible for them. Grant Agreement N° 101096923.

varying term that sums the noise bounds implicitly after they are mapped through the nonlinear autonomous term $f(z_k) = f(y_k, d_k)$ via interval arithmetic. The term $h_w(\bar{w})$ bounds the uncertainties of the model, while $G(\cdot)$ denotes the input map of the system, $H = [I_n - I_n]^\top \in \mathbb{R}^{2n}, I_n \in \mathbb{R}^{n \times n}$ is the identity matrix of dimension n.

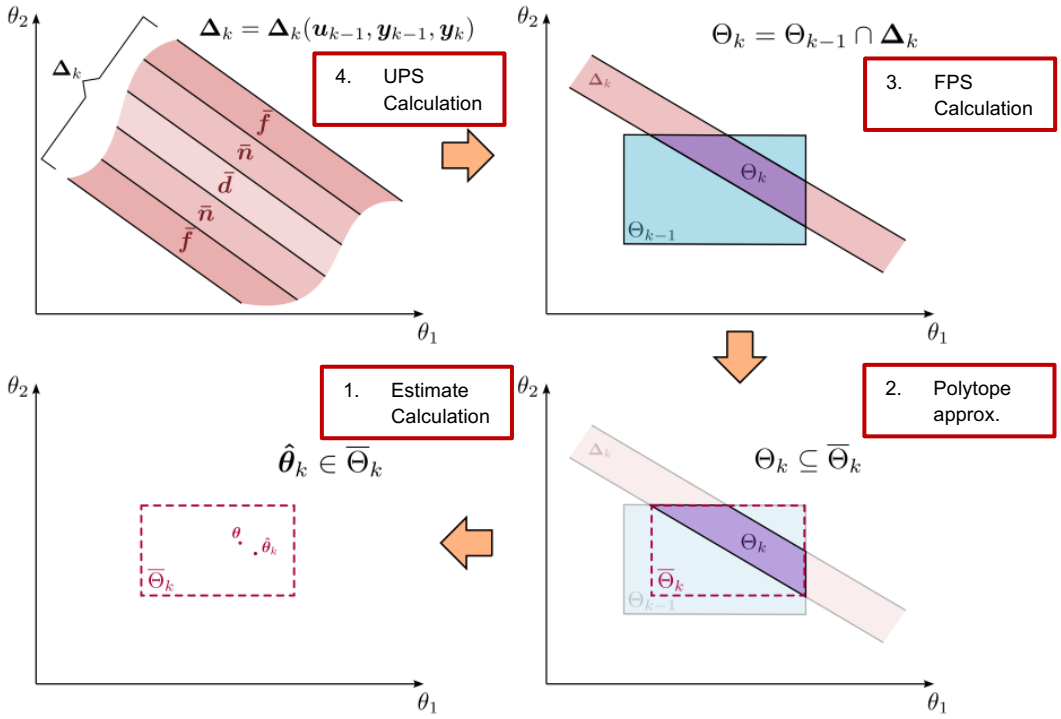

Figure 5 Overview of the different steps in SME in a 2-D example (adapted from Tsolakis, et al., 2024b).

The computation of the Feasible Parameter Set consists of the following steps (Tsolakis, et al., 2024b):

1) Recursively compute a set of predefined, normalized directions, $E = \{e_1, e_2, \dots\}$, normal to the faces of the outer-approximating polytope. These directions are based on the number of parameters p and a user-defined accuracy iterator ϕ. This is computed offline.

2) Compute the new FPS $\Theta_k = \Theta_{k-1} \cap \Delta_k$ based on the outer-approximation of the previous time step and the new UPS computed at time k starting with $\overline{\Theta}_0 = \Theta_0$.

3) Compute the set of vertices $V_k = \{v_k^1, v_k^2, \dots\}$ of the convex polytope $\boldsymbol{\Theta} k$.

4) Compute the outer approximation Θ_k of the convex polytope Θ_k based on the set of vertices V_k and the set of predefined directions.

5) Go back to Step 2.

Funded by the European Union

Funded by the European Union. Views and opinions expressed are however those of the author(s) only and do not necessarily reflect those of the European Union or CINEA. Neither the European Union nor CINEA can be held responsible for them. Grant Agreement N° 101096923.

3.2.2 Parameter estimate

The final step is to derive an estimate $\hat{\theta}_k$ for the unknown parameter θ_k that belongs to the derived parameter set $\bar{\theta}_k$. We can exploit here the fact that the system is linear to the parameters of interest and use the following equation (Tsolakis, et al., 2024b):

$$G(u_{k-1})\theta = y_k - f(y_{k-1}), \tag{29}$$

which is a linear algebraic equation to the unknown parameter θ_k and where the disturbance and the noise are included in the measurement. If we concatenate (29) for the last N_m measurements, to leverage more data, we can get a regression equation (Tsolakis, et al., 2024b):

$$\Phi \cdot \theta = \xi, \tag{30}$$

where θ here is the regress and, $\Phi = \left[G\left(u_{k-1-N_m}\right), \dots, G(u_{k-1})\right]^\top$ is the regressor and $\xi = \left[y_{k-N_m} - f(y_{k-1-N}), \dots, y_k - f(y_{k-1})\right]^\top$ the observation. Solving this equation at every time step renders the estimation $\hat{\theta}$.

3.2.3 SME-based Fault Diagnosis

Under healthy conditions, the actual parameter θ_k lies in both UPS and FPS, implying the intersection of the two sets. However, if $\bar{\Theta}_{k-1} \cap \Delta_k = \emptyset$, then a fault is guaranteed to be detected. A fault is detected at the first timestep k_D when the following condition occurs (Tsolakis, et al., 2024b):

$$k_D = min_k(\bar{\Theta}_{k-1} \cap \Delta_k = \emptyset, k > k_F), \tag{31}$$

where k_F indicates that the timestep that a fault has occurred. To isolate the fault, we follow a similar approach as for the detection, but now we need to check the projection of the FPS on the different principal axes of the parameter space first. The projection of the FPS on the principal axes of the parameter space is given by (Tsolakis, et al., 2024b):

$$Proj_{\theta_i}(\Theta_k) = \left[\min_{v \in \mathcal{V}}\left(e_{\theta_i}^\top v\right), \min_{v \in \mathcal{V}}\left(e_{\theta_i}^\top v\right)\right], \tag{32}$$

where $e_{\theta_i}, i = 1, 2, \dots, p$ denotes the unit vectors of the orthonormal basis of the parameter space, and $v \in \mathcal{V}$ represents the vertices of the FPS. Since the FPS is a convex set by construction, this one-dimensional projection results in an interval. We can then compare these intervals before and after fault detection. If $Proj_{\theta_i}(\Theta_k) \cap Proj_{\theta_i}(\Theta_{k_D-1}) = \emptyset$, then θ_i is guaranteed to be faulty.

A fault is isolated at the first timestep $k_I^i, i = 1, 2, \dots, p$ when the following condition occurs (Tsolakis, et al., 2024b):

$$k_I^i = \min_{\mathrm{k}}\left(Proj_{\theta_i}(\Theta_k) \cap Proj_{\theta_i}\left(\Theta_{k_D-1}\right) = \emptyset, k > k_D\right). \tag{33}$$

Following fault detection and isolation, the parameter set is reinitialized and begins to converge toward a “faulty" FPS, accompanied by a new estimate for the fault parameters.

Funded by the European Union

Funded by the European Union. Views and opinions expressed are however those of the author(s) only and do not necessarily reflect those of the European Union or CINEA. Neither the European Union nor CINEA can be held responsible for them. Grant Agreement N° 101096923.

4 AUTONOMOUS GNC SCHEME DEVELOPMENT

In this Chapter, the development process of the GNC scheme, applicable to both Short-Sea an Inland Waterway operations, is discussed. The GNC system decisions are managed by a higher-level Risk control layer. In the context of project SEAMLESS, this layer features a POMDP (Partially Observable Markov Decision process) model-based risk mitigation framework and a Bayesian Belief Network (BBN), outlined in Figure 6, **with the details presented in the SEAMLESS registered publication (Dhyani, Wang, et al., 2024).** The BBN computes the transition probabilities for the POMDP model. Inputs from various metrological and communication sources, such as onboard sensors, Automatic Identification System (AIS), electronic navigational charts (ENC), metocean services, and sensor monitoring agents are required for this purpose. The POMDP model provides risk mitigation support in the form of a Safe Control Strategy (SCS), prompting the vessel into a safe state, i.e., a minimum risk condition (MRC). The SCS suggests the use of a fail-safe or fail-operational action. For instance, the following actions are proposed in the case of Inland Waterway Transport (IWT) (Dhyani, Wang, et al., 2024):

1) Fail-safe strategies
    a) $A_{r,1}$: “Limp home”
    b) $A_{r,3}$: “Keep position and heading (DP control strategy is selected)”
    c) $A_{r,5}$: “Move away from the quay and other vessels”
2) Fail-operational strategies
    a) $A_{r,2}$: “Fault-tolerant control strategy is selected”
    b) $A_{r,4}$: “Human supervision is requested”
    c) $A_{r,6}$: “Vessel’s speed is reduced”

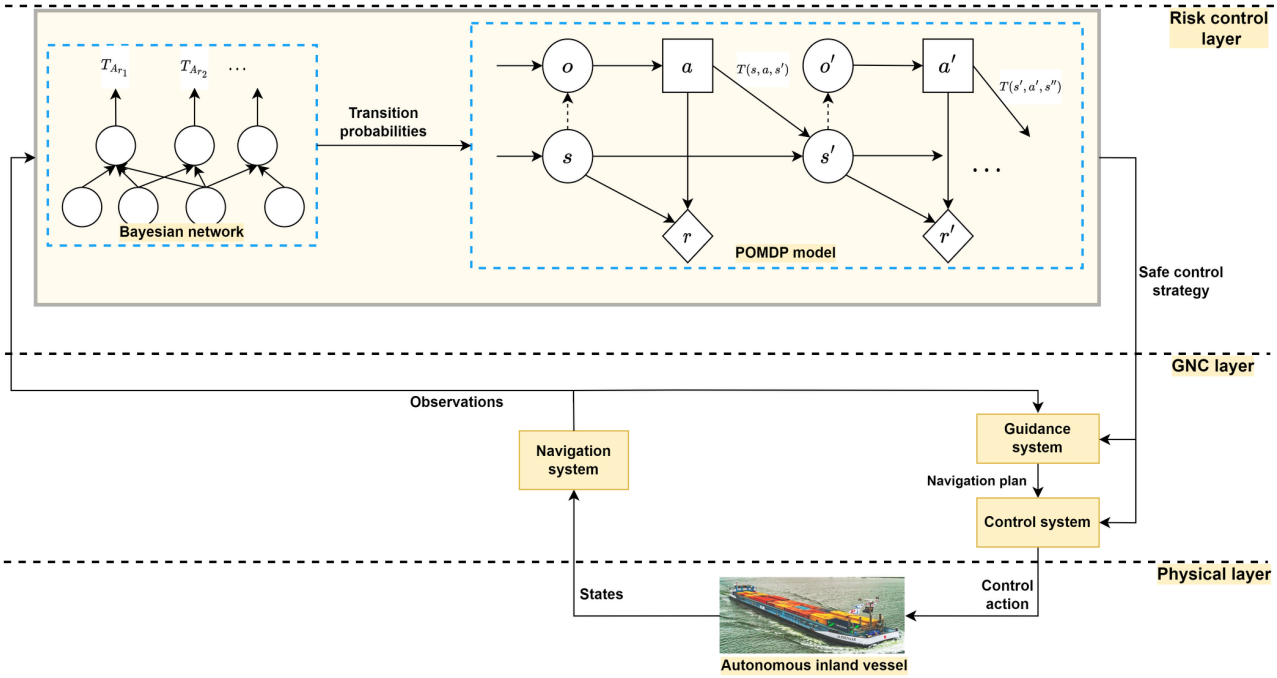

Figure 6 Online risk mitigation scheme for autonomous inland vessels and connection to GNC system (Dhyani, et al., 2024b).

Funded by the European Union

Funded by the European Union. Views and opinions expressed are however those of the author(s) only and do not necessarily reflect those of the European Union or CINEA. Neither the European Union nor CINEA can be held responsible for them. Grant Agreement N° 101096923.

The proposed GNC design integrates awareness to both COLREGs and regional (e.g., BPR) traffic rules (Chapter 2) with semantic reasoning functions, to increase the safety of ASVs, when carrying out their navigational objectives. Interfacing with the monitoring agents, described in Chapter 3, allows for fault-tolerant capabilities. The following sections will thus report on the fault-tolerant ($A_{r,2}$) and collision-free ($A_{r,5}$) path planning actions, as well as the semantic reasoning capabilities. **Parts of the relevant research are featured as part of the SEAMLESS registered publications (Kougiatsos et al., 2026; Kougiatsos & Reppa, 2026).**

4.1 Fault-Tolerant and Collision-Free Path Planning

Assuming a continuous path curve C consisting of n waypoints $(x_k, y_k)^\top$, $k = 1, \cdots, n$, with $x_k \in \mathbb{R}$, $y_k \in \mathbb{R}$ denoting planar coordinates, as shown in Figure 7, the path-tangential reference frame is rotated by an angle (Kougiatsos & Reppa, 2026):

$$\psi_k = atan2(x_{k+1} - x_k, y_{k+1} - y_k), \forall k \in 1,2, \dots, n \tag{34}$$

with the function $atan2\ (x, y)$ returning the angle between the positive x-axis of the plane and the point given by coordinates (x, y) on it.

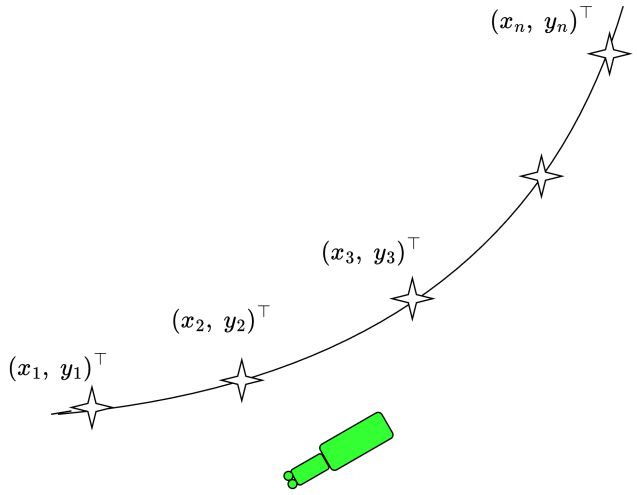

Figure 7 Definition of the Path following objective.

When the own ASV is located at a point $(y_{\zeta,1}, y_{\zeta,2})^T$, defined by the position measurements $y_{\zeta,1}$ (longitude measurement) and $y_{\zeta,2}$ (latitude measurement), its cross-track error e is defined as the orthogonal distance between the vessel's position and the tangential path, which renders the following mathematical expression (Fossen, 2023; Kougiatsos & Reppa, 2026):

$$e(t) = -\underbrace{\left(y_{\zeta,1}(t) - \hat{f}_1(t) - x_k\right)}_{\boldsymbol{x-position\ error}} cos(\psi_k) + \underbrace{\left(y_{\zeta,2}(t) - \hat{f}_2(t) - y_k\right)}_{\boldsymbol{y-position\ error}} sin(\psi_k), \tag{35}$$

Funded by the European Union

Funded by the European Union. Views and opinions expressed are however those of the author(s) only and do not necessarily reflect those of the European Union or CINEA. Neither the European Union nor CINEA can be held responsible for them. Grant Agreement N° 101096923.

where $k \in \{0, \cdots, n\}$ chosen to represent the following waypoint from the current position of the vessel, and $\hat{f}_i$, $i = 1, 2$ denotes the estimation of the x-position ($i = 1$) and y-position ($i = 2$) sensor faults, respectively. The fault estimation is essential for ensuring the fault tolerance in the guidance. Measurements from the GNSS sensor (latitude, longitude), the gyrocompass/ dual-channel GNSS (heading) are required for the implementation of the estimator. The Speed Over Ground (SOG) of the vessel can be obtained either by AIS data, or by former GNSS positions (Fossen, 2022), thus limiting the need for further redundancy in hardware sensors. The minimum required sensors are collectively denoted as $\mathcal{S}$ in Figure 8. The estimation process further requires information related to the diagnosed faults. As shown in Figure 8, this data is provided by the monitoring agents, with the relevant design specifications explained in Chapter 3.

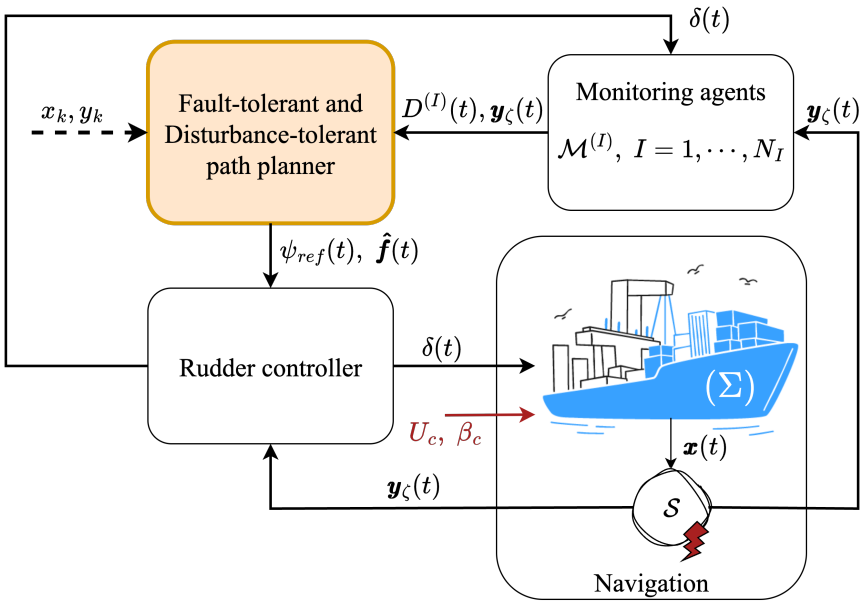

Figure 8 Integration of the monitoring agents in the GNC scheme and fault accommodation using virtual sensors (Kougiatsos & Reppa, 2026).

More specifically, an ALOS guidance law is designed to reduce the cross-tracking error e, defined in (35), by providing suitable reference heading angle ψ_{ref} signals to the controller. The guidance law is able to mitigate the sensor fault effects and the effects of drift-inducing external disturbances (e.g., currents), and is defined as (Fossen, 2023; Kougiatsos & Reppa, 2026):

$$\psi_{ref} = \psi_k - atan\left(\frac{e}{X_D} + \hat{\beta}\right), \tag{36}$$

where X_D is the lookahead distance (typically assuming values between $1.5L - 3L$, L is the length of the vessel, $\hat{\beta} \in \mathbb{R}$ is the estimate of the unknown slip angle. To this end, the following nonlinear adaptive estimator formulation applies (Kougiatsos & Reppa, 2026):

$$\dot{\hat{x}}_\zeta = \gamma(\hat{x}_\zeta, u) + \Lambda(y_\zeta - \hat{x}_\zeta - \hat{f}) + \Omega\dot{\hat{f}}, \tag{37}$$

$$\dot{\Omega} = -\Lambda, \tag{38}$$

Funded by the European Union

Funded by the European Union. Views and opinions expressed are however those of the author(s) only and do not necessarily reflect those of the European Union or CINEA. Neither the European Union nor CINEA can be held responsible for them. Grant Agreement N° 101096923.

$$\dot{\hat{\beta}} = \Gamma_1 \frac{U_r \cdot X_D}{\sqrt{{X_D}^2 + (e + X_D \cdot \beta)^2}} e, \tag{39}$$

$$\dot{\hat{f}} = \Gamma_2 (\Omega + 1) D\left[y_\zeta - \hat{x}_\zeta - \hat{f}\right], \tag{40}$$

where $\hat{x} = [\hat{x}_1, \hat{x}_2, \hat{x}_3]^T$ contains the estimates of the position and heading states, $\Lambda \in \mathbb{R}^3$ denotes the nonlinear estimator gains , $\Gamma_1 \in \mathbb{R}$ and $\Gamma_2 \in \mathbb{R}^3$ are the learning rates of the adaptive laws in (39) and (40), respectively and $\hat{f} \in \mathbb{R}^3$ are the estimates of unknown sensor faults. A filtering term $\Omega \in \mathbb{R}^3$ is added to ensure the stability of the state-equation adaptive scheme. Finally, $D[\cdot]$ is the dead-zone operator, used to activate the sensor fault identification, given as (Kougiatsos et al., 2026):

$$D\left[y_\zeta - \hat{x}_\zeta - \hat{f}\right] = \begin{cases} 0, if\ D^{(I)} = 0 \\ y_\zeta - \hat{x}_\zeta - \hat{f}, if\ D^{(I)} = 1 \end{cases}. \tag{41}$$

To avoid collisions, the waypoints $k + 1,\ k = 1, \dots, N$ at each timestep t need to be modified using the terms $\left(\delta x_{k+1}(t), \delta y_{k+1}(t)\right)^T$, so that the new path is defined as (Kougiatsos et al., 2026):

$$\begin{cases} x'_{k+1}(t) = x_{k+1} + \delta x_{k+1}(t), \\ y'_{k+1}(t) = y_{k+1} + \delta y_{k+1}(t), \end{cases} \tag{42}$$

where $x'_{k+1}(t)$ and $y'_{k+1}(t)$ denote the coordinates of the modified reference path. The following sections are used to derive conditions, relevant to $\left(\delta x_{k+1}(t), \delta y_{k+1}(t)\right)^T$, for collision avoidance with both other vessels and the surrounding infrastructure.

4.1.1 Avoiding collisions with other vessels

The assessment of the encounter conditions between the own vessel and other vessels typically involves performing several geometrical calculations using sensor measurements to assess quantities such as the relative bearing and relative heading between the own and other vessels, the distance between the own and other vessel(s) d and the distance between the own vessel and the bank (d_l). Based on the various applicable traffic rules (i.e., COLREGS, BPR, PRR), “ample time” should be allowed to make decisions related to collision avoidance, while the vessels are expected to “keep well clear” of each other. In the majority of literature works, these requirements geometrically translate to an encounter distance ρ_{enc}, used to initiate the assessment of the encounter situation when other vessels are in range of this radius, and a safe distance ρ_s, used to enforce the vessels to keep well clear of each other (Hu et al., 2022),. Moreover, a vessel radius $\rho_p = L/2$ and $\rho_q = L'/2$ is prescribed for the own and other vessel, respectively, where L' denotes the length of the other vessel. The relative bearing ψ_β is used to characterize the relative position between the two vessels, while the relative heading ψ_c characterizes the difference in the heading of the two vessels. The formulas used for the calculation of ψ_β , ψ_c can be found in (Tsolakis et al., 2024).

If the current position $\left(x_{o,i}, y_{o,i}\right)^\mathsf{T}$ and heading $\psi_{o,i}$ of each of the other vessels i $(i = 1, 2, \cdots, N_v)$ is known (e.g., using a combination of GNSS coupled with AIS data), where N_v denotes the total

Funded by the European Union

Funded by the European Union. Views and opinions expressed are however those of the author(s) only and do not necessarily reflect those of the European Union or CINEA. Neither the European Union nor CINEA can be held responsible for them. Grant Agreement N° 101096923.

number of the other vessels, we can deduce that the other vessels' movement at every following time step t is constrained on the lines (Kougiatsos et al., 2026):

$$\mathcal{E}_i: y'_{o,i}(t) = y_{o,i} + \left(x'_{o,i}(t) - x_{o,i}\right)\tan\left(\psi_{o,i}\right), \tag{43}$$

where $\left(x'_{o,i}(t), y'_{o,i}(t)\right)^{\mathsf{T}}$ denotes the future estimated positions of the other vessel $i = 1, \dots, N_v$. For each new future waypoints $k+1$ of the own vessel, we calculate its distance from each $\mathcal{E}_i$ according to the following formula (Kougiatsos et al., 2026):

$$d_{W,\mathcal{E}_i}(t) = \frac{\left|y'_{k+1} + \left(x_{o,i} - x'_{k+1}(t)\right)\tan\left(\psi_{0,i}\right) - y_{o,i}\right|}{\sqrt{1 + \tan^2\psi_{o,i}}}, \forall i \in 1,2,\cdots, N_v. \tag{44}$$

To guarantee a vessel-to-vessel collision-free path, our vessel should maintain a safe distance ρ_s from every other vessel that allows for "ample time for decision-making", meaning that (Kougiatsos et al., 2026):

$$d_{W,\mathcal{E}_i}(t) \geq \rho_p + \rho_q + \rho_s, \tag{45}$$

which after some algebraic manipulations renders the following set of conditions (Kougiatsos et al., 2026):

$$|\delta y_{k+1} - \delta x_{k+1} tan(\psi_{o,i})| \geq (\rho_s + \rho_p + \rho_q)\sqrt{1 + \tan^2(\psi_{o,i})}\,1 +$$

$$\left|(y_{o,i} - y_{k+1}) + (x_{k+1} - x_{o,i})tan(\psi_{o,i})\right|, \forall i \in \{1, \dots, Nv\}. \tag{46}$$

In Figure 9 conditions (46) bound the displacement of the own vessel (blue) waypoints to keep clear from each other vessel (green), by a distance greater than a certain threshold (green/ dashed line).

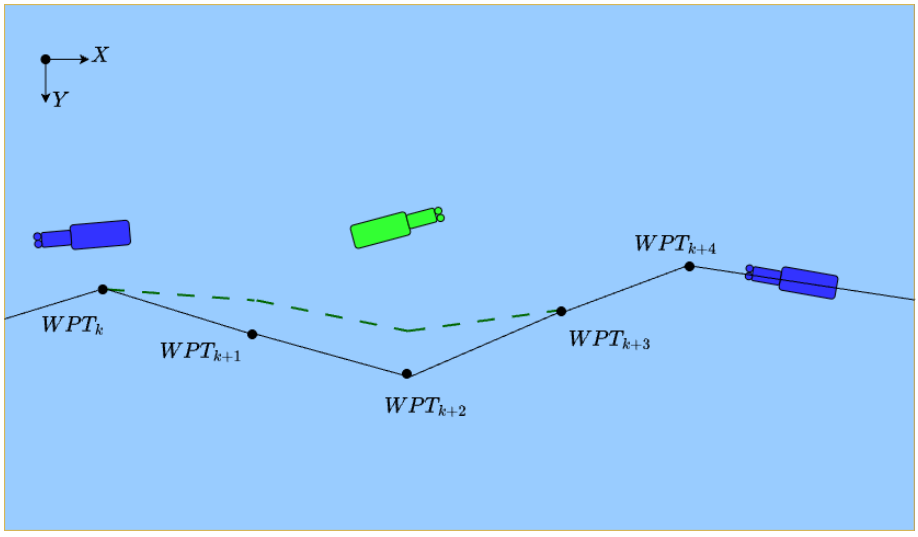

Figure 9 Envelope of collision-free vessel trajectories, considering other traffic participants.

Funded by the European Union

Funded by the European Union. Views and opinions expressed are however those of the author(s) only and do not necessarily reflect those of the European Union or CINEA. Neither the European Union nor CINEA can be held responsible for them. Grant Agreement N° 101096923.

4.1.2 Avoiding collisions with infrastructure

During navigation, a certain safe distance needs to be respected from the physical limits (e.g., bank) of the waterway. For instance, Rule 9 of COLREGS dictates that “A vessel proceeding along the course of a narrow channel or fairway shall keep as near to the outer limit of the channel or fairway which lies on her starboard side as is safe and practicable [...]”.

Let us define $(x, y) \rightarrow w$, as the non-constant but known waterway width on the planar coordinates of our vessel, and s_w as a safety factor defining the safe distance from the bounds of the canal and receiving values in $[0, 1]$. This factor serves as a heuristic, and its value can be set for limiting vessel-to-bank interactions (Lataire et al., 2018). Smart Buoy systems have been amongst the research interests of the European Union for the past years, through union-wide and regional projects, such as CRISTAL (Fraunhofer CML, 2025) and “Safe beach zones” (Dimitrov et al., 2025), respectively. These buoys inform the guidance system decisions using their transmitted GNSS sensor position data, as follows. Assuming that the position of each buoy $j = 1, \cdots, N_B$, where N_B is the total number of buoys, scattered throughout the waterway or the shore, denoted as $\left(x_{B,j}, y_{B,j}\right)^{\mathrm{T}}$ is known, we can define a line, passing between two consecutive buoys $\{j, j+1\}$ as (Kougiatsos et al., 2026):

$$\mathcal{E}_j : y'_{B,j} = y_{B,j} + \left(x'_{B,j} - x_{B,j}\right) \frac{y_{B,j+1} - y_{B,j}}{x_{B,j+1} - x_{B,j}}, \tag{47}$$

where $\left(x'_{B,j}, y'_{B,j}\right)^{\mathrm{T}}$ are the coordinates of each point that lies on $\mathcal{E}_j$. For each of the new future waypoints $k+1$ of the own vessel, we calculate its distance from $\mathcal{E}_j$ according to the following formula (Kougiatsos et al., 2026):

$$d_{W,\mathcal{E}_i}(t) = \frac{\left| y'_{k+1} + \left(x_{B,j} - x'_{k+1}(t)\right) \frac{y_{B,j+1} - y_{B,j}}{x_{B,j+1} - x_{B,j}} - y_{B,j} \right|}{\sqrt{1 + \left(\frac{y_{B,j+1} - y_{B,j}}{x_{B,j+1} - x_{B,j}}\right)^2}}, \forall j \in 1,2,\cdots, N_B. \tag{48}$$

The clearance requirement to the waterway banks can then be mathematically translated as (Kougiatsos et al., 2026):

$$(1 - s_w)w \geq d_{W,\mathcal{E}_j}(t) \geq s_w w, \tag{49}$$

which after some algebraic manipulations renders the following constraints (Kougiatsos et al., 2026):

$$\left| \delta y_{k+1} - \delta x_{k+1} \cdot \frac{y_{B,j+1} - y_{B,j}}{x_{B,j+1} - x_{B,j}} \right| \leq (1 - s_w)w \sqrt{1 + \left(\frac{y_{B,j+1} - y_{B,j}}{x_{B,j+1} - x_{B,j}}\right)^2}$$

$$- \left| y_{k+1} + \left(x_{B,j} - x_{k+1}\right) \frac{y_{B,j+1} - y_{B,j}}{x_{B,j+1} - x_{B,j}} - y_{B,j} \right|, \tag{50}$$

Funded by the European Union

Funded by the European Union. Views and opinions expressed are however those of the author(s) only and do not necessarily reflect those of the European Union or CINEA. Neither the European Union nor CINEA can be held responsible for them. Grant Agreement N° 101096923.

$$\left|\delta y_{k+1} - \delta x_{k+1} \cdot \frac{y_{B,j+1} - y_{B,j}}{x_{B,j+1} - x_{B,j}}\right| \geq s_w w \sqrt{1 + \left(\frac{y_{B,j+1} - y_{B,j}}{x_{B,j+1} - x_{B,j}}\right)^2}$$

$$+ \left|y_{k+1} + \left(x_{B,j} - x_{k+1}\right)\frac{y_{B,j+1} - y_{B,j}}{x_{B,j+1} - x_{B,j}} - y_{B,j}\right|, \forall j \in 1,2,\cdots,N_B \quad (51)$$

When the risk of collision exists for the own ASV and it assumes a Give Way (GW) or Emergency Give Way (EGW) role, potential collisions with other vessels and the available infrastructure can be avoided, if the planned waypoints are horizontally and vertically displaced in the earth-fixed frame by $\delta x_{k+1}(t) \in \mathbb{R}$ and $\delta y_{k+1}(t) \in \mathbb{R}$, respectively, abiding by the constraints (46), (50) and (51). This implies a collision-free envelope for the own vessel, dependent on the traffic conditions and evolving over time, where the risk of collision is eliminated. An example of a collision-free envelope is illustrated in Figure 10, with the green dashed and purple dashed lines representing the lower and upper bound of the envelope, respectively.

The various traffic rules also determine the specifics of the behavior that the vessels should adopt to avoid collisions. For instance, for head-on encounters, COLREGS mention that the vessels should take appropriate action to pass each other port to port. This can be translated in terms of δx_{k+1}, δy_{k+1}, and added as a preference to the envelope as (Kougiatsos et al., 2026):

$$\delta y_{k+1}(t) \cdot \delta x_{k+1}(t) \leq 0 \quad (52)$$

At each time t, the smallest possible trajectory deviation would be preferred. This translates to an optimization problem, formulated as follows (Kougiatsos et al., 2026):

$$\min_{\delta x_{k+1},\ \delta y_{k+1}} \{\delta x_{k+1},^2 + \delta y_{k+1}^2\}, \qquad \forall\, k = 0, \dots, N-1 \quad (53)$$

subject to:

Collision-free envelope

- $Eq.(46) \forall i \in \{1,2, \dots, N_v\}$
- $Eq.(50) \forall j \in (1,2, \dots, N_B)$
- $Eq.(51) \forall\, j \in (1,2, \dots, N_B)$
- $Eq.(52)$

Funded by the European Union

Funded by the European Union. Views and opinions expressed are however those of the author(s) only and do not necessarily reflect those of the European Union or CINEA. Neither the European Union nor CINEA can be held responsible for them. Grant Agreement N° 101096923.

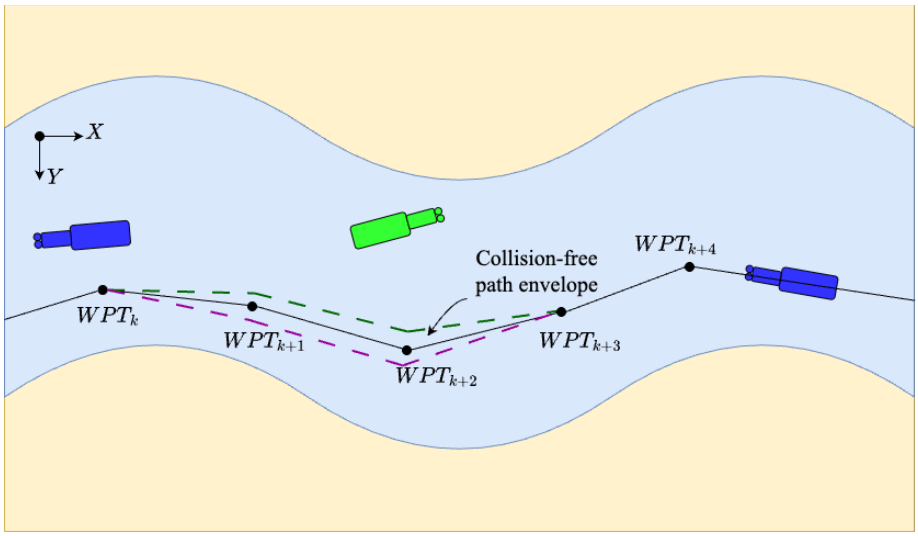

Figure 10 Envelope of collision-free vessel trajectories, considering other traffic participants, and the infrastructure limitations.

4.2 SEMANTIC REASONING CAPABILITIES

During operation, the **selection of the applicable traffic rules** from the semantic database takes the form of a mapping using the GNSS signal measurement, as follows (Kougiatsos et al., 2026):

$$\mathcal{Y}_{GNSS} \times \mathcal{F} \mapsto \mathcal{F}^s, \tag{54}$$

where $\mathcal{Y}_{GNSS}$ denotes the space of GNSS sensor measurements and $\mathcal{F}^s = \mathcal{F}_e^s \cup \mathcal{F}_r^s \subseteq \mathcal{F}$ denotes the applicable part of the semantic database to the current traffic situation.

The **traffic roles** for the traffic participants are assigned using the Finite-State Machine Approach presented in Chapter 2. To this end, the geometrical parameters of the encounter situation, like the relative bearing ψ_β , the relative heading ψ_c and the lane distance are fed by the semantic reasoner to the Finite-State Machine. The approach also requires information on $\mathcal{F}^s$, to choose between the two branches in Figure 3. More specifically, the COLREGs branch applies to Short-Sea environments and the regional regulations (e.g., BPR) branch applies to Inland Waterways.

In cases where the own vessel assumes a Give-Way or an Emergency Give-Way role, **appropriate action needs to be taken to avoid collisions**. The action to avoid collisions that is considered in the design of the semantic reasoner is that of changing the reference trajectory of future waypoints that the own vessel should follow (see $\mathrm{A}_{\mathrm{r},5}$), based on the method described in Section 5.1. This change occurs during operation and is updated at every following time step, until the encounter situation is resolved. When one or multiple faults affect the sensors of the ASV, their timely detection by the monitoring agents, discussed in Chapter 3, allows for the activation of fault tolerant capabilities (see $\mathrm{A}_{\mathrm{r},2}$), outlined in Section 5.1.

Funded by the European Union

Funded by the European Union. Views and opinions expressed are however those of the author(s) only and do not necessarily reflect those of the European Union or CINEA. Neither the European Union nor CINEA can be held responsible for them. Grant Agreement N° 101096923.

5 USE CASES

This Chapter presents some practical use cases for the SEAMLESS solutions developed in the context of WP4, Task 4.2, and presented through the course of this deliverable. Some of them are targeted at the use of a single proposed solution, while others combine multiple of the presented solutions.

The presented Use Cases are constructed to clearly show the fulfilment of the promises made in the Grant Agreement, by the methods designed in Chapters 2-4.

- The management of "remedial actions (e.g. by reconstructing the faulty sensor information using virtual sensors, or by using virtual actuators to reconstruct the actions, or by adapting the controller)" is illustrated through an IWT example in Use Case 1.
- "The monitoring module" capabilities in "(i) detecting local fault occurrence, (ii) isolating the fault type (e.g. sensor fault, engine fault) and/or location (e.g. radar sensor fault, GNSS sensor fault), (iii) distinguishing between local faults and falsified communicated data (e.g. spoofing of AIS data) and propagated faults", is showcased through Use Cases 2 and 3.
- Use Case 4 presents the fault-tolerant capabilities of the GNC scheme applied to Demo Use Case 1 (DUC1) of SEAMLESS.
- "COLREG-compliance" alongside "the effect of COLREGs alterations on this predicament" are showcased in Case study 5, involving operation in a mix of IWT and SSS.

5.1 CASE STUDY 1: RISK MITIGATION FOR AN INLAND WATERWAY SCENARIO

In this section, a case study is conducted to illustrate the performance of the proposed POMDP model-based framework, briefly introduced in Chapter 4, in terms of "managing" different "remedial actions" to ensure safety. In the considered scenario, a fault affects the onboard GNSS sensor and is diagnosed by the vessel's sensor monitoring module (see Chapter 3). The considered Inland Waterway Transport (IWT) environment is characterized by rough weather conditions and moderate traffic. All other conditions are assumed to be in a moderate or medium state.

The BBN computes the output risk probabilities, considering various Risk Influencing Factors (RIFs), including but not limited to the traffic density, navigational sensors health and weather conditions. To discourage excessive dependence on remote or onboard crew intervention, as part of the calculation of the state transition probabilities, higher rewards are assigned to fail-operational actions than those reading to fail-safe actions. In addition, a penalty is assigned to transitions leading the vessel to remain in the same state for the subsequent time step. This prevents stagnant behavior and promotes a prompt transition to a safe state (i.e, MRC). The POMDP model is initialized at the unsafe state S_{u_1}(i.e., "vessel does not follow the desired path"), as a result of taking action A_{u_1}(i.e., "R&T commands provided based on incorrect vessel's navigational states, leading to the vessel being unable to follow the planned path."). The initial state belief is set at S_{u_1} (i.e., "Vessel does not follow the desired path"), and the Monte Carlo Tree Search runs until a terminal state (i.e., safe state) is reached. In most of the algorithm run cases, the simulation ends after 2 epochs (i.e, 2000 simulation runs), whereas in the rest of cases, the simulation ends after 1 epoch (i.e., 1000 simulation runs). Nonetheless, a safe state is reached successfully in all algorithm's runs, with the following SCSs for the hazardous situations selected:

Funded by the European Union

Funded by the European Union. Views and opinions expressed are however those of the author(s) only and do not necessarily reflect those of the European Union or CINEA. Neither the European Union nor CINEA can be held responsible for them. Grant Agreement N° 101096923.

(1) S_{u_2} : "Keep position (DP control strategy is selected)" (A_{r_3})
(2) S_{u_3} : "Vessel's speed is reduced" (A_{r_6})

The reader can find more information on the considered probabilities, RIFs and the obtained results in the SEAMLESS registered publication (Dhyani, et al., 2024).

5.2 Case Study 2: Sensor Fault Diagnosis Capabilities of the Monitoring Agent

In this section, the monitoring agent prototype, presented in Chapter 3, is simulated for a sensor fault case affecting the vessel's navigational sensors. **The relevant results and analysis are featured in the SEAMLESS registered publication (Dhyani, et al., 2024)**.

The case study considers the navigation of the "Tito-Neri" model vessel, developed at TU Delft, along a predefined trajectory to evaluate the effectiveness of the proposed FDI approach. The hydrodynamic model parameters are provided in (Bruggink et al., 2018). Wind effects are considered in the simulation with a velocity of $V = 2\,m/s$ and an angle of $\beta_V = 45\,deg$, coming from the southwest direction.

The navigation system is simulated for 3000 seconds. The fault detection observer gain matrices $K^{(1)}, K^{(2)}, K^{(4)}$ are taken to be equal to a diagonal matrix $diag([100, 100, 100])$, and $K^{(3)}$ is equal to 100. Each sensor is corrupted by Gaussian noise, having an amplitude within 3% of the mean absolute value of the noiseless sensor measurement. Further, the design parameters for the adaptive thresholds in each of the monitoring modules are selected as follows: $\rho^{(1,1)} = \rho^{(1,2)} = \rho^{(2,1)} = 0.001$; $\xi^{(1,1)} = \xi^{(1,2)} = \xi^{(2,1)} = 1$; $\rho_d^{(1,1)} = \rho_d^{(1,2)} = \rho_d^{(2,1)} = 10$; $\xi_d^{(1,1)} = \xi_d^{(1,2)} = \xi_d^{(2,1)} = 1$; $\rho^{(2,2)} = 1$, $\xi^{(2,2)} = 95$, $\rho_d^{(2,2)} = 0.1$, $\xi_d^{(2,2)} = 4$.

The theoretical fault signatures used in the aggregator module are provided in Table 2, where, $F_{c_1} = \{f_p\}$, $F_{c_2} = \{f_\psi\}$, $F_{c_3} = \{f_v\}$, $F_{c_4} = \{f_p, f_\psi\}$, $F_{c_5} = \{f_p, f_v\}$, $F_{c_6} = \{f_\psi, f_v\}$ and $F_{c_7} = \{f_p, f_\psi, f_v\}$. Given the structure of the FSM matrix, any combination of faults can be isolated, which can be further verified by simulating different fault scenarios.

Table 2 Sensor fault signature matrix for the aggregator $\mathcal{A}$ (Dhyani, et al., 2024)

	F_{c_1}	F_{c_2}	F_{c_3}	F_{c_4}	F_{c_5}	F_{c_6}	F_{c_7}
$\varepsilon_{y_\zeta}^{(1,1)}$	1	*	0	1	1	*	1
$\varepsilon_{y_\zeta}^{(1,2)}$	0	1	0	1	0	1	1
$\varepsilon_{y_\zeta}^{(2,1)}$	0	1	1	1	1	1	1
$\varepsilon_{y_\zeta}^{(2,2)}$	0	0	1	0	1	1	1

Permanent faults in the gyrocompass and GNSS sensors occur at $T_{f_\psi} = 500\,sec$ and $T_{f_p} = 1500\,sec$, during the considered scenario. The residual signals and the corresponding adaptive thresholds for the j-th sensor monitored by $M^{(I)}$ are plotted under $M^{(I,j)}$ in Figure 11. As shown, the residuals corresponding to the gyrocompass (in $M^{(1,2)}$ and $M^{(2,1)}$) exceed the thresholds at $t =$

Funded by the European Union

Funded by the European Union. Views and opinions expressed are however those of the author(s) only and do not necessarily reflect those of the European Union or CINEA. Neither the European Union nor CINEA can be held responsible for them. Grant Agreement N° 101096923.

$500\ sec$, whereas, the residuals corresponding to the GNSS (in $M^{(1,1)}$) exceed the thresholds at $t = 1500\ sec$. For $t < 500\ sec$, the components of the detection vectors $D(t)$ remain zero, and the diagnosis set corresponds to a null set. For $500 \leq t < 1500\ sec$, the occurrence of the first fault is detected by the residual exceeding the adaptive threshold, which results in $D(t) = [0\ 1\ 1\ 0]^{\mathrm{T}}$. For $t \geq 1500\ sec$, the second fault is detected, leading to $D(t) = [1\ 1\ 1\ 0]^{\mathrm{T}}$. At the end of the simulation, a consistency test is performed by comparing the observed pattern $D(t)$ to the theoretical patterns F_{c_q}, which results in a diagnosis set $\mathcal{D}_s(t) = \{F_{c_2}, F_{c_4}\} = \{\{f_\psi\}, \{f_p, f_\psi\}\}$, thereby isolating the faulty sensors.

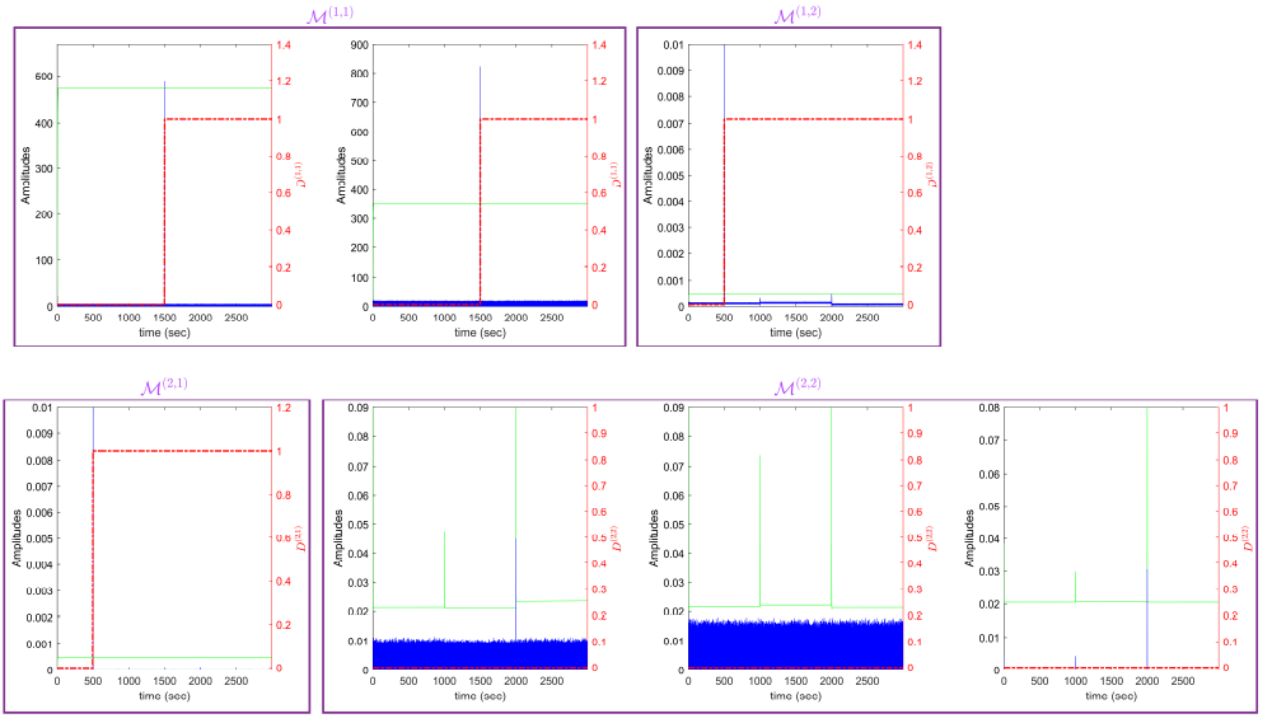

Figure 11 Simulation results of the residual signals, the corresponding adaptive thresholds, and the decision vectors for each monitoring module (Dhyani, et al., 2024).

5.3 Case Study 3: Actuator Fault Diagnosis Capabilities of the Monitoring Agent

This section presents the results of the monitoring agent prototype application, introduced in Chapter 3, for an ASV navigation case facing actuator faults. **The relevant results and analysis are featured as part of the SEAMLESS registered publication (Tsolakis, et al., 2024b).**

In the considered scenario, the ASV follows a sinusoidal reference path, having access to full-state measurements, corrupted by uniformly bounded noise. The disturbances are also considered uniformly bounded, with known bounds. Figure 12 illustrates the evolution of two different FPSs at six equidistant time instances. The FPS using the proposed UPS formulation and accounting for measurement noise is shown in blue. The FPS from the existing UPS formulation without considering measurement noise is shown in orange. The blue FPS is feasible under healthy conditions, monotonically converging towards a “healthy area" around the healthy value $\theta = (1\ 1\ 1)^{\mathrm{T}}$, while

Funded by the European Union

Funded by the European Union. Views and opinions expressed are however those of the author(s) only and do not necessarily reflect those of the European Union or CINEA. Neither the European Union nor CINEA can be held responsible for them. Grant Agreement N° 101096923.

preventing false alarms. In contrast, the orange FPS becomes infeasible, preventing consistent convergence to the “healthy area" and triggering false alarms.

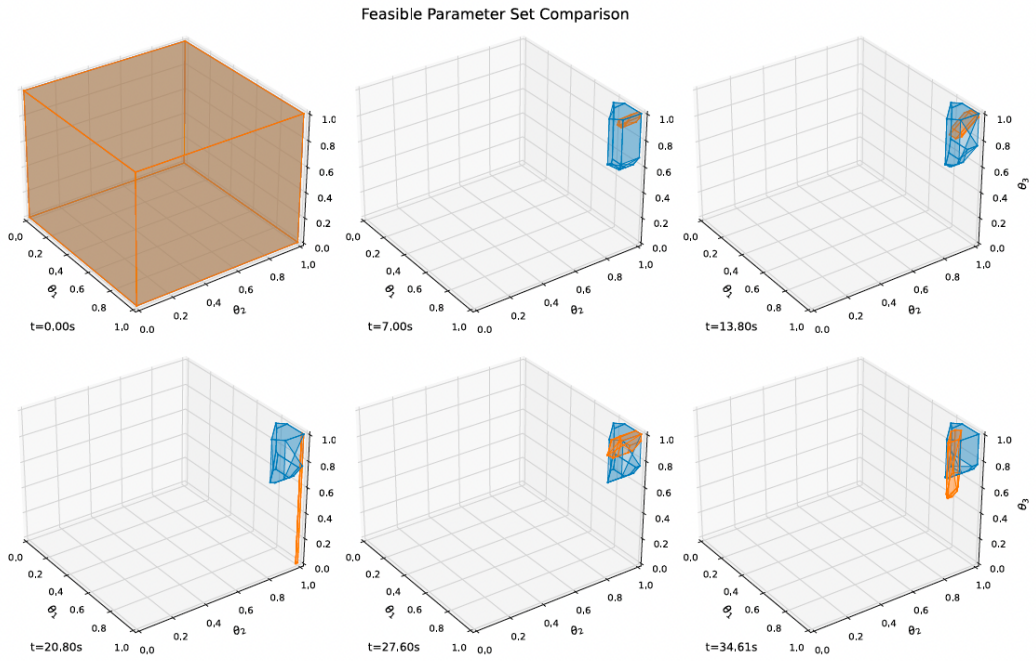

Figure 12 Evolution of the FPS in healthy conditions. In blue, the FPS considers measurement noise, converging towards the “healthy" region. In contrast, the orange FPS, which neglects noise, becomes infeasible multiple times and fails to converge uniformly (Tsolakis, et al., 2024b).

The ASV is also simulated in a straight, horizontal reference path-following scenario while avoiding collisions with other vessels (assuming COLREGs apply). The system is subjected to both disturbance and noise and at time $t_F = \Delta t k_f = 20s$, a permanent fault $\theta_r = 0.2$ is injected in the right thruster. Different outer approximations of the FPS are compared and evaluated based on their sensitivity, while a comparison of the regularized parameter estimate proposed in Chapter 3 with the conventional one is performed. Both FPSs are constructed from UPSs that account for measurement noise. Figure 13 shows the evolution of the FPS using two different outer approximations. A “tighter" outer approximation with $\phi = 1$, and a “looser" approximation with $\phi = 0$ are presented with cyan and pink lines respectively. At time $t = 20.41sec$, after the fault occurs, the cyan approximation leads to an infeasible set, indicating fault detection, as it starts converging towards a “faulty area". The pink approximation also converges towards the faulty region, delayed due to its larger volume.

The parameter estimates are shown in Figure 14. More specifically, the regularized parameter estimate is displayed in cyan, followed by the un-regularized estimate displayed in pink. The corresponding FPS bounds are shown in matching colours. The moment of the fault is marked by a red dashed vertical line. The fault is detected at $t = 20.56\ sec$ using the tighter approximation (blue dashed vertical line) and at t = $21\ sec$ using the looser approximation (purple dashed vertical line). The regularized parameter estimate (cyan continuous line) is generally more stable than the unregularized one (pink continuous line), making it a more reliable nominal estimate to evaluate the true fault value.

Funded by the European Union

Funded by the European Union. Views and opinions expressed are however those of the author(s) only and do not necessarily reflect those of the European Union or CINEA. Neither the European Union nor CINEA can be held responsible for them. Grant Agreement N° 101096923.

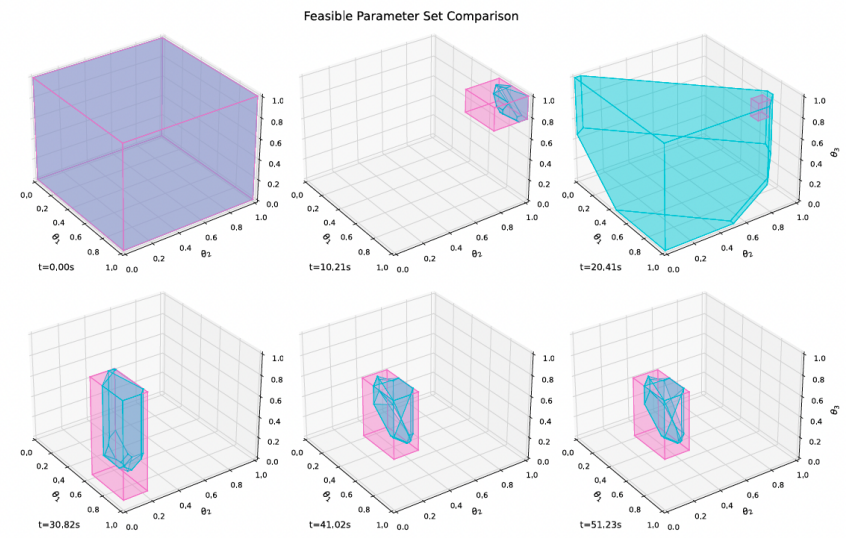

Figure 13 Comparison of the FPS evolution using two different outer approximations. The top-right sub-figure highlights the moment just after the fault occurs. The tighter outer approximation (cyan) detects the fault faster and begins to converge toward the faulty region, while the looser approximation (pink) converges more slowly (Tsolakis, et al., 2024b).

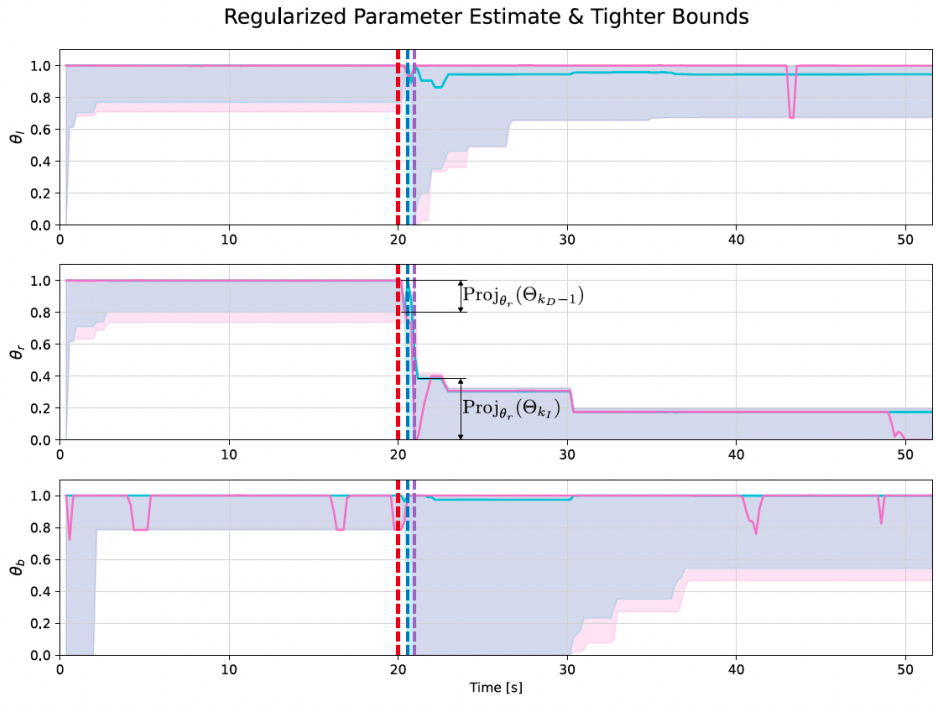

Figure 14 Parameter estimate with corresponding bounds (shaded areas). In the second sub-plot for θ_r , the discontinuity in FPS bounds indicates the fault in the right thruster. The fault occurs at the red dashed vertical line, with the detection time shown in purple. The regularized estimate (cyan) is more stable and closer to the true value compared to the unregularized estimate (pink) (Tsolakis, et al., 2024b).

Funded by the European Union

Funded by the European Union. Views and opinions expressed are however those of the author(s) only and do not necessarily reflect those of the European Union or CINEA. Neither the European Union nor CINEA can be held responsible for them. Grant Agreement N° 101096923.

5.4 CASE STUDY 4: FAULT-TOLERANT CAPABILITIES IN THE NORTHERN EUROPEAN USE CASE

To showcase the efficiency and performance of the guidance system developed in Chapter 4 in the presence of sensor faults, diagnosed by the monitoring agent in Chapter 3, a case study of the Ro/Ro cargo vessel MARIT travelling a parabolic route between the areas of Horten and Moss (Norway) is used. **The follow-up results and analysis are featured as part of the SEAMLESS registered publication (Kougiatsos & Reppa, 2026).**

The actual routes (red and green colors) and the translation of the red one in a computer-based simulation are shown in Figure 15. The total travel time for this route is approximately $T = 50min$. The principal dimensions and characteristics of the MARIT vessel are shown in Table 3. Regarding the used model parameters, commonly referred to as the hydrodynamic coefficients, these were estimated using empirical relations identified in (Abkowitz, 1980) and the data of Table 3.

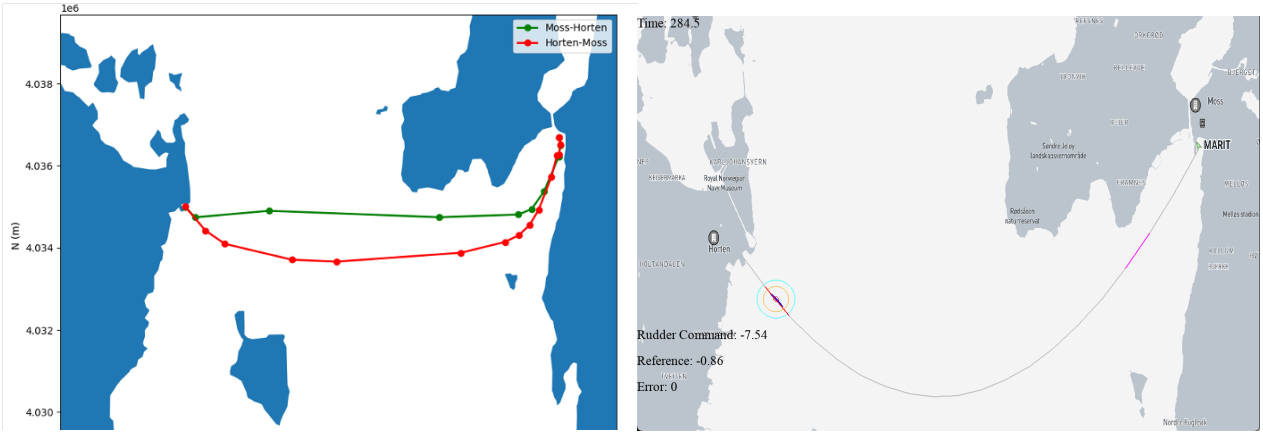

Figure 15 Routes of the ASKO vessel MARIT, used in the SEAMLESS North European Demonstration, between Horten and Moss, shown on the left. The red route is used in this Case study and inserted in the simulation environment, as shown on the right.

Table 3 Principal dimensions and characteristics of the RO/RO cargo vessel MARIT operating between Horten and Moss (Kougiatsos & Reppa, 2026).

Dimension	Value	Description [Units]
L	67	Length $[m]$
B	15	Beam $[m]$
T	1.6	Design draft $[m]$
C_b	0.3	Block coefficient $[-]$
U	8	Speed $[kn]$

The ASV operation is simulated under the occurrence of a sensor fault, affecting the heading angle measurement $y_\zeta\{3\}$. The magnitude of the fault is chosen as $f\{3\} = 1\,rad$, with its time of occurrence at $t_1 = 1200\,sec\ (\approx 20min)$. The sensor measurements are corrupted by uniformly bounded sensor noise $\bar{d}$ of 3 % magnitude. Ocean currents affect the vessel's velocities with a magnitude of $U_c = 0.02\,m/sec$ and an angle of $\beta_c = 26\,deg$. To account for the unknown drift due to the effects from the ocean currents and the lack of speed measurements, as well as the

Funded by the European Union

Funded by the European Union. Views and opinions expressed are however those of the author(s) only and do not necessarily reflect those of the European Union or CINEA. Neither the European Union nor CINEA can be held responsible for them. Grant Agreement N° 101096923.

occurrence of sensor faults, the guidance law (37) - (40) is designed with the following parameters: $\Lambda = [2,2,2]^{\mathrm{T}}, \Gamma_1 = 10^{-6}, \Gamma_2 = [400,400,400]^{\mathrm{T}}, X_D = 200\,m.$

A PID reference heading tracking controller is designed for path following, with the rudder angle δ updated for this purpose, similar to (Fossen, 2023) :

$$\delta(t) = u(t) = K_p\left(\tilde{\psi}(t) + \frac{1}{T_i}\int_0^t \tilde{\psi}(t)\,dt + T_d\,\dot{\tilde{\psi}}(t)\right), \tag{55}$$

where $\tilde{\psi}(t) = \psi_{ref}(t) - y_\zeta\{3\}(t) - \hat{f}\{3\}(t)$ is the heading angle tracking error at time step t, ψ_{ref} is calculated by (36), $\hat{f}\{3\}$ is estimated by (40), $K_p = 80$ is the controller's proportional gain, $T_d = 10$ and $T_i = 0.5$ are the derivative and integral time constants, respectively.

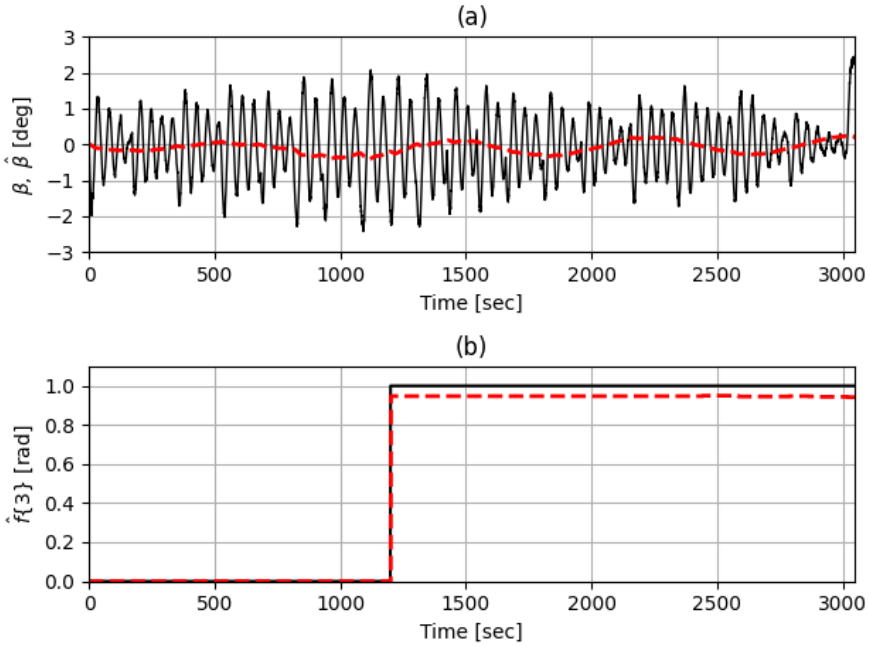

Figure 16 Estimates of **(a)** the unknown sideslip angle $\hat{\beta}$ using (42), and **(b)** the sensor fault $\hat{f}\{3\}$ using (43) and comparison with actual values. The estimates are styled in red and dashed lines, while the actual values are shown in black, continuous lines (Kougiatsos & Reppa, 2026).

The simulation results regarding the adaptive estimation process and the achieved cross-tracking error are shown in Figures 16 and 17, respectively. Further quantification results are provided in Table 4, such as the mean value and standard deviation of the derived error signals. Figure 16(a) illustrates the adaptive estimation of the unknown sideslip angle β, shown in black colour/ continuous line, by the adaptive estimator $\hat{\beta}$ designed in (39), and shown in red colour/dashed line. As observed in this Figure, the estimation can follow the trend of the actual unmeasured sideslip angle, though unable to catch its peaks. Nonetheless, the estimation error remains rather small, with a mean of $-0.02\,deg$, and a standard deviation of $1.15\,deg$, as recorded in Table 4. Similarly, Figure 16(b) showcases the adaptive estimation of the inserted sensor fault $f\{3\}$, shown in black color/ continuous line, by the adaptive estimator $\hat{f}\{3\}$ designed in (40), and shown in red colour/dashed line.

Funded by the European Union

Funded by the European Union. Views and opinions expressed are however those of the author(s) only and do not necessarily reflect those of the European Union or CINEA. Neither the European Union nor CINEA can be held responsible for them. Grant Agreement N° 101096923.

Satisfactory estimation results are obtained with a mean error of $-0.03\ rad$ and a standard deviation of $0.03\ rad$, in Table 4.

Table 4 Performance Indicators related to the fault-tolerant capabilities described in Chapter 4 (Kougiatsos & Reppa, 2026)

Parameter	Indicator	Value
e	Mean	0.17 m
	Std	4.6 m
$f\{3\} - \hat{f}\{3\}$	Mean	0.03 rad
	Std	0.03 rad
$\beta - \hat{\beta}$	Mean	-0.02 deg
	Std	1.15 deg

To showcase the efficiency of the path following capabilities, Figure 17 presents the calculation of the cross-tracking error e, defined in Chapter 4. For the most part of the simulation, e remains confined between the values of $-10\,m \approx -67\% \cdot B$ and $10\,m \approx 67\% \cdot B$, with two peaks outside this margin close to the time $t_1 = 1200\ sec$ of insertion of the simulated sensor fault. A mean error value of $0.17\,m$ with a standard deviation of $4.6\,m$ is recorded in Table 4, advocating for the resilience of the developed Guidance system against sensor faults and environmental disturbances.

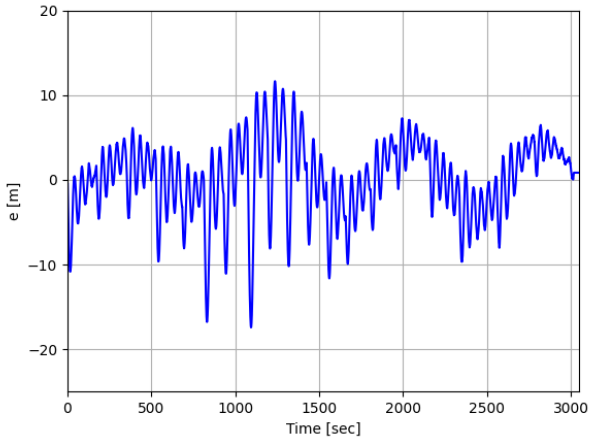

Figure 17 Calculation of cross-tracking error e during the vessel's operation, using (38) (Kougiatsos & Reppa, 2026).

5.5 Case Study 5: Collision-free Capabilities In Different Traffic Environments

In this section, the results from the application of the collision-free path planning in multi-environment operations developed in Chapter 4 are presented. To this end, a Pusher-Barge ASV case study is employed operating between a short-sea and a Dutch inland waterway environment. The principal dimensions and parameters of the ASV model have been already provided in (C. Zhang et al., 2025). **The follow-up results and analysis are featured as part of the SEAMLESS registered publication (Kougiatsos et al., 2026).**

Funded by the European Union

Funded by the European Union. Views and opinions expressed are however those of the author(s) only and do not necessarily reflect those of the European Union or CINEA. Neither the European Union nor CINEA can be held responsible for them. Grant Agreement N° 101096923.

The sensor measurements are corrupted by uniformly bounded random sensor noise, with $|d| \leq \bar{d}$. The PID reference heading tracking controller from (55) is applied with $K_p = 80$ is the controller's proportional gain, $T_d = 10$ and $T_i = 1$ are the derivative and integral time constants, respectively.

For the simulation purposes, the own vessel is tasked to follow a reference route starting at $(x, y) = (100, 0)^\top$ and finishing at $(x, y) = (6000, 0)^\top$, discretized in $N = 20$ evenly spaced waypoints. During the mission, the own vessel encounters $N_v = 2$ opposite-moving Pusher-Barge vessels, posing risks for head-on collisions. The encounter between the own vessel and vessel $i = 1$ occurs at the short-sea environment, where the other vessel $i = 1$ starts from the point $(x_{o,1}, y_{o,1}) = (2400, 0)^\top$. The encounter between the own vessel and vessel $i = 2$ occurs in the Dutch Inland waterway environment, where the other vessel $i = 2$ starts from the point $(x_{o,2}, y_{o,2}) = (6000, 0)^\top$. The waterway has a fixed width $w = 750m$ and the safety clearance factor from the banks is taken as $s_w = 0.2$. Based on previous results of experiments related to ship-to-ship interaction (Vantorre et al., 2002), a minimum value for the safe distance ρ_s between the vessels equal to $0.5B$ is assumed, where B is the own vessel's breadth. This choice of value is shown to minimize the lateral force and yaw moment between the vessels during head-on and overtaking encounter situations. A value of $\rho_{enc} = 6L \approx 600m$ is assumed for the encounter distance of the own vessel. To capture the effects of regulations in the path planner for the head-on scenario, Rules 6-8, 14, 16, 17, and 18 of COLREGS and Articles 6.03, 6.04, and 6.07 of BPR are semantically described in $\mathcal{F}$.

Assuming a noise level $\bar{d} = 3\%$, Figure 18(a) illustrates the difference between the achieved distance between the own vessel and vessel $i \in \{1, 2\}$, denoted as d_i and the safe distance ρ_s. More specifically, the difference $d_1 - \rho_s$ is shown with blue color/ continuous line, while the difference $d_2 - \rho_s$ is shown with magenta/ dash-dotted line. Both curves turn out to be positive, which signifies that vessels stay clear from each other, respecting the safe distance. The time windows of the two head-on encounters are highlighted, based on the defined ρ_{enc}. The lane distances $d_l^{(p)}$ and $d_l^{(s)}$ from the banks of the waterway are shown in Figure 18(b) for both the own vessel (blue and red/ continuous lines) and vessel $i = 2$ (purple and orange/ dash-dotted lines). All curves are bounded according to (49), where the upper and lower bounds are illustrated with green/ dashed lines. As a result, the clearance requirement from the banks of the waterway is indeed well respected.

Figure 19 illustrates the time histories of the heading angles corresponding to the three simulated vessels for the case study. As shown in this Figure, the own vessel (blue line) and other vessel $i = 1$ (green line) both make evasive manoeuvres to avoid collision in the first encounter time-window (translated from Figure 18(a)), with $y_\zeta\{3\}$ dropping below 0 deg and $\psi_{o,1}$ assuming values between 120 and 180 deg. As a result, the two vessels pass each other port to port, as described in COLREGs, before starting to correct their headings again to their original values, following the first encounter time window. The own vessel continues with almost zero heading in the inland waterway environment, where it meets the other vessel $i = 2$ (heading drawn in purple) coming from the opposite direction. This encounter happens in the second time- window, also translated from Figure 18(a). According to Figure 18(b), the distance of the own vessel from the starboard side bank (red continuous line) is less than the distance of the other vessel $i = 2$ from the same bank (orange dash-dotted line). As a result, the own vessel follows the starboard side of the waterway. Based on

Funded by the European Union

Funded by the European Union. Views and opinions expressed are however those of the author(s) only and do not necessarily reflect those of the European Union or CINEA. Neither the European Union nor CINEA can be held responsible for them. Grant Agreement N° 101096923.

Rule 6.04 of BPR, the modular Finite State Machine in Figure 3 assigns the SO role to the own vessel. Symmetrically, the other vessel $i = 2$ assumes a GW role and should take action to avoid collision. The appropriate action for vessel $i = 2$ is to alter its reference path in such a way as to pass the own vessel port to port, illustrated by the reduction of the heading angle between 160 deg and 180 deg. The own vessel proceeds on its original course, not needing to take action to avoid collision. Thus, the two vessels resolve the head-on encounter scenario as defined in the BPR rules.

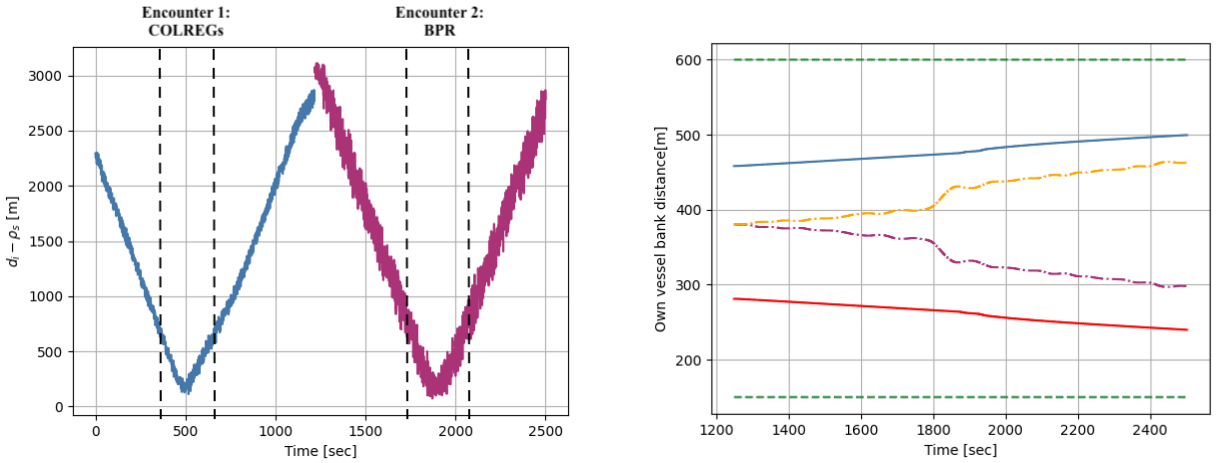

(a) **(b)**

Figure 18 **(a)** Distance between the own vessel and other vessel $i = 1$ (d_1 shown in blue), and between the own vessel and other vessel $i = 2$ (d_2 shown in purple), and **(b)** distance between own vessel and the waterway banks (blue/red continuous lines), and between other vessel i = 2 and the waterway banks (orange/purple dash-dotted lines). The bounds in (49) are shown with green/ dashed lines (Kougiatsos et al., 2026).

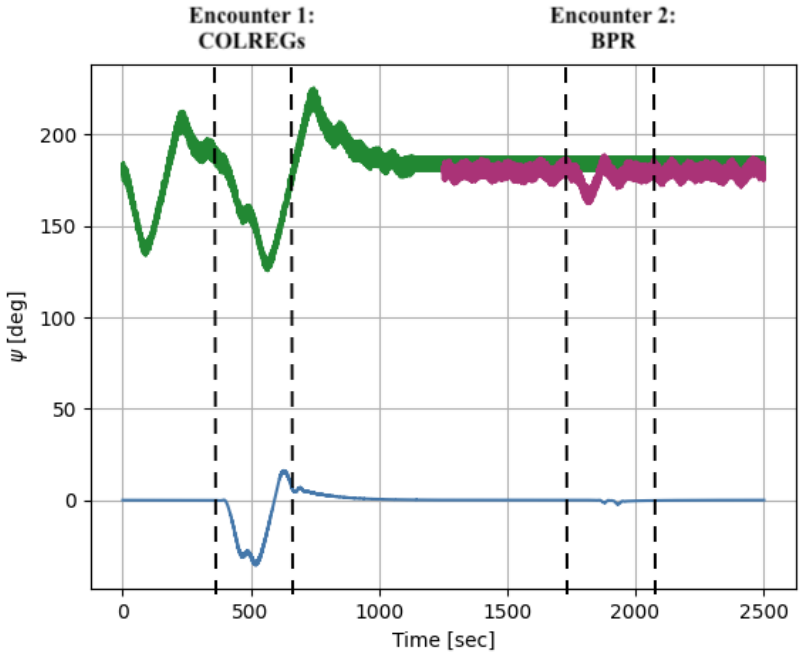

Figure 19 Time history of the recorded heading angles for the own vessel (blue), other vessel $i = 1$ (green), and other vessel $i = 2$ (purple), in the defined simulation scenario (Kougiatsos et al., 2026).

Funded by the European Union

Funded by the European Union. Views and opinions expressed are however those of the author(s) only and do not necessarily reflect those of the European Union or CINEA. Neither the European Union nor CINEA can be held responsible for them. Grant Agreement N° 101096923.

6 CONCLUSIONS

6.1 MAIN RESULTS

This deliverable presented solutions related to the Autonomous GNC scheme development and monitoring agent prototype. Rule awareness was achieved using a semantic database and a modular Finite-State Machine, in Chapter 2, transcribing the parameters corresponding to the operational environment and to both international and regional traffic rules in a computer-cognitive format. An online framework based on a POMDP approach, briefly discussed in Chapter 4, is responsible for the mitigation of navigational risks through proper decision making on the strategies to follow. More specifically, two types of strategies were identified: the fail-operational and the fail-safe strategies.

The **fail-operational strategies** correspond to a joint need for action by the monitoring agent and the guidance system of the vessel to mitigate the risks. In those cases, the monitoring agent is used to detect and isolate the occurrence of multiple sensor and/or actuator faults affecting the navigation. Model-based residual generation and adaptive threshold computation, as well as Set-Membership Estimation are used for this purpose, as discussed in Chapter 3. Following the fault diagnosis, fault-tolerant capabilities can be used to restore the health of the navigation system components, such as the virtual-sensor informed guidance law presented in Chapter 4.

The **fail-safe strategies** mostly concern operation under healthy system conditions, with external forces of risks (e.g., collision risks posed by other traffic participants) being most prevalent. In those cases, the vessel may be required to modify her original trajectory to mitigate the collision risk. Chapter 4 discussed the generation of a collision-free envelope, considering both other vessels (dynamic obstacles) and the surrounding infrastructure (static obstacles). Collision avoidance is executed following the applicable traffic rule guidelines, selected by the semantic reasoner.

The obtained results from the case studies in Chapter 5 highlighted the individual strengths but also the matching between the different proposed solutions. Considering DUC1 of SEAMLESS, that is the Northern European Use Case, the combination of the monitoring agent prototype with the virtual sensor-enhanced guidance allowed for minimal cross-tracking error in the presence of sensor faults and external disturbances. The collision-avoidance behaviour was shown to adapt to the relevant traffic rules when switching from a short-sea environment, where COLREGS apply, to a Dutch inland waterway environment, where BPR applies. The inland waterway scenario where the risk mitigation method was applied highlights the associated navigational risks and favourable strategies.

6.2 CONNECTION WITH SEAMLESS SOLUTIONS AND KEY PERFORMANCE INDICATORS

The methods presented in this work have the potential to work alongside and boost the performance of other important SEAMLESS solutions, such as the low-attention Remote Operation Center (ROC) architecture and ModalNET. The reason for that are the collision-free and fault-tolerant capabilities, which would allow for higher system uptime, less attention by remote operators, and fewer disruptions in the waterway traffic network (i.e., due to the avoidance of accidents).

To enable multi-environment operations, this deliverable considered both international (COLREGS) and regional (BPR) traffic rules. Rule awareness was enabled using a semantic database, populated

Funded by the European Union

Funded by the European Union. Views and opinions expressed are however those of the author(s) only and do not necessarily reflect those of the European Union or CINEA. Neither the European Union nor CINEA can be held responsible for them. Grant Agreement N° 101096923.

with information on the operational environment characteristics and traffic rule requirements and, a modular Finite-state machine matching the various encounter scenarios to the traffic roles assumed by the vessels, in Chapter 2. Future amendments, if needed, to the traffic rules can easily get reflected in the design of the database and Finite State Machine. These tools are also scalable and could potentially incorporate more regional regulations (e.g., PRR), as well as different requirement (e.g., design) standards. Our aspiration is for the ASV operation to more closely follow updates in requirements for approval purposes. To this end, the embedded rule awareness contributes to **SEAMLESS KPI 2.2: "Reduce general cost and time required for approving deployment of autonomous ships by at least 75%"**.

The development of a monitoring agent prototype, able to diagnose both sensor and actuator faults in a timely manner enables the inclusion of fault-tolerant capabilities in the GNC scheme. By employing virtual sensors in the decision-making of the Guidance system, sensor fault effects can be automatically mitigated, and the operation resumes as intended. Moreover, the online navigational risk mitigation framework discussed in Chapter 4 ensures that at least one minimum risk condition of the vessel is reached until the remote operator(s) are available to intervene in the decision-making of the system. As a result, this deliverable contributes to **SEAMLESS KPI 2.3: "Reduce workload for ROC operators, ships per operator > 1"**. The proposed solutions contribute to the SEAMLESS vision of safe, intelligent, and autonomous waterborne transport.

7 REFERENCES

Abkowitz, M. A. (1980). *MEASUREMENT OF HYDRODYNAMIC CHARACTERISTICS FROM SHIP MANEUVERING TRIALS BY SYSTEM IDENTIFICATION*.

AS, D. N. V. G. L. (2018). *Classification Guideline DNVGL-CG-0264: Autonomous and Remotely Operated Ships*.

Baldini, A., Felicetti, R., Freddi, A., Longhi, S., & Monteriù, A. (2022a). Actuator fault tolerant control via active fault diagnosis for a remotely operated vehicle. *IFAC-PapersOnLine*, *55*(6), 310–316.

Baldini, A., Felicetti, R., Freddi, A., Longhi, S., & Monteriù, A. (2022b). Fault tolerant control for remotely operated vehicles with thruster faults using nonlinear disturbance observers. *IFAC-PapersOnLine*, *55*(31), 275–280.

Blanke, M. (2006). *Fault-tolerant Sensor Fusion for Marine Navigation*. Elsevier.

Bolbot, V., Theotokatos, G., Wennersberg, L. A., Faivre, J., Vassalos, D., Boulougouris, E., Jan Rødseth, Ø., Andersen, P., Pauwelyn, A. S., & Van Coillie, A. (2023). A novel risk assessment process: Application to an autonomous inland waterways ship. *Proceedings of the Institution of Mechanical Engineers, Part O: Journal of Risk and Reliability*, *237*(2), 436–458. https://doi.org/10.1177/1748006X211051829

Bruggink, D., Cremer, Q., Groenewegen, R., & Klokgieters, A. (2018). *Differentiation of maneuvering coeffi- cients for scaled model vessels*.

Funded by the European Union

Funded by the European Union. Views and opinions expressed are however those of the author(s) only and do not necessarily reflect those of the European Union or CINEA. Neither the European Union nor CINEA can be held responsible for them. Grant Agreement N° 101096923.

Bryne, T. H., Fossen, T. I., & Johansen, T. A. (2017). Design of inertial navigation systems for marine craft with adaptive wave filtering aided by triple-redundant sensor packages. *International Journal of Adaptive Control and Signal Processing*, *31*(4), 522–544.

Chen, X., Yao, W., Chi, R., & Cui, Z. (2024). MFALC Control of Aquaculture Vessel Based on Improved ILOS Guidance Law. *2024 IEEE 13th Data Driven Control and Learning Systems Conference (DDCLS)*, 601–604.

ClassNK. (2020). *Guidelines for Automated/ Autonomous Operation on ships (Ver. 1.0)*.

Cocquempot, V., Izadi-Zamanabadi, R., Staroswiecki, M., & Blanke, M. (1998). Residual generation for the ship benchmark using structural approach. *UKACC International Conference on Control (CONTROL'98)*, 1480–1485.

Commission Centrale pour la Navigation du Rhin (CCNR). (2024). *Règlement de police pour la navigation du rhin (RPNR)*.

Convention on the International Regulations for Preventing Collisions at Sea, 1972 ARTICLE I General Obligations ARTICLE II Signature, Ratification, Acceptance, Approval and Accession. (n.d.).

Corradini, M. L., Monteriù, A., & Orlando, G. (2011). An actuator failure tolerant control scheme for an underwater remotely operated vehicle. *IEEE Transactions on Control Systems Technology*, *19*(5), 1036–1046. https://doi.org/10.1109/TCST.2010.2060199

Cristofaro, A., & Johansen, T. A. (2014). Fault tolerant control allocation using unknown input observers. *Automatica*, *50*(7), 1891–1897.

Dhyani, A., Negenborn, R. R., & Reppa, V. (2024). A Multiple Sensor Fault Diagnosis Scheme for Autonomous Surface Vessels. *IFAC-PapersOnLine*, *58*(4), 31–36. https://doi.org/10.1016/j.ifacol.2024.07.189

Dhyani, A., Wang, Y., Verbeke, M., Pissoort, D., & Reppa, V. (2024). A POMDP model-based online risk mitigation method for autonomous inland vessels. *IFAC-PapersOnLine*, *58*(20), 335–340.

Dimitrov, I., Iliev, I., Hristov, D., Dinkov, D., & Mavrodiev, T. (2025). Design and Implement an Automatic Smart Buoy System for a Bulgarian Safe Beach Areas – Part 1. *TransNav, the International Journal on Marine Navigation and Safety of Sea Transportation*, *19*(2), 381–386. https://doi.org/10.12716/1001.19.02.05

European Maritime Safety Agency. (2025). *Annual Overview of Marine Casualties and Incidents 2025*.

Fenton, N., & Neil, M. (2019). *Risk Assessment and Decision Analysis with Bayesian Networks* (2nd ed.). CRC Press (Taylor & Francis Group).

Funded by the European Union

Funded by the European Union. Views and opinions expressed are however those of the author(s) only and do not necessarily reflect those of the European Union or CINEA. Neither the European Union nor CINEA can be held responsible for them. Grant Agreement N° 101096923.

Fossen, T. I. (2022). Line-of-sight path-following control utilizing an extended Kalman filter for estimation of speed and course over ground from GNSS positions. *Journal of Marine Science and Technology*, *27*(1), 806–813.

Fossen, T. I. (2023). An adaptive line-of-sight (ALOS) guidance law for path following of aircraft and marine craft. *IEEE Transactions on Control Systems Technology*, *31*(6), 2887–2894.

Fossen, T. I., & Aguiar, A. P. (2024). A uniform semiglobal exponential stable adaptive line-of-sight (ALOS) guidance law for 3-D path following. *Automatica*, *163*. https://doi.org/10.1016/j.automatica.2024.111556

Fraunhofer CML. (2025, December 2). *Expert interview with Björn Krämer and Tammo Märtens "We Want to Enhance Navigability for Tributaries."* Https://Www.Fraunhofer.de/En/Press/Research-News/2025/December-2025/We-Want-to-Enhance-Navigability-for-Tributaries.Html.

Freddi, A., Longhi, S., & Monteriù, A. (2013). Actuator fault detection system for a remotely operated vehicle. *IFAC Proceedings Volumes*, *46*(33), 356–361.

Gu, N., Wang, D., Peng, Z., Wang, J., & Han, Q.-L. (2022). Advances in line-of-sight guidance for path following of autonomous marine vehicles: An overview. *IEEE Transactions on Systems, Man, and Cybernetics: Systems*, *53*(1), 12–28.

Hashemi, M., & Shami, E. (2021). New fault detection and fault-tolerant scheme for Doppler velocity logger outage in ocean navigation systems. *The Journal of Navigation*, *74*(2), 409–424.

He, Y., Liu, X., Zhang, K., Mou, J., Liang, Y., Zhao, X., Wang, B., & Huang, L. (2022). Dynamic adaptive intelligent navigation decision making method for multi-object situation in open water. *Ocean Engineering*, *253*, 111238.

Hinostroza, M. A., Xu, H., & Guedes Soares, C. (2021). Motion planning, guidance, and control system for autonomous surface vessel. *Journal of Offshore Mechanics and Arctic Engineering*, *143*(4), 41202.

Hu, L., Hu, H., Naeem, W., & Wang, Z. (2022). A review on COLREGs-compliant navigation of autonomous surface vehicles: From traditional to learning-based approaches. In *Journal of Automation and Intelligence* (Vol. 1, Issue 1). KeAi Communications Co. https://doi.org/10.1016/j.jai.2022.100003

Kepaptsoglou, K., Fountas, G., & Karlaftis, M. G. (2015). Weather impact on containership routing in closed seas: A chance-constraint optimization approach. *Transportation Research Part C: Emerging Technologies*, *55*, 139–155. https://doi.org/https://doi.org/10.1016/j.trc.2015.01.027

Kougiatsos, N., Dhyani, A., & Reppa, V. (2026). Integrating Rule Awareness and Semantic Reasoning in Collision-Free Vessel Path Planning. *Submitted to IFAC World Congress 2026 as a Dual Journal-Conference Submission (under Review)*.

Funded by the European Union

Funded by the European Union. Views and opinions expressed are however those of the author(s) only and do not necessarily reflect those of the European Union or CINEA. Neither the European Union nor CINEA can be held responsible for them. Grant Agreement N° 101096923.

Kougiatsos, N., & Reppa, V. (2026). Virtual Sensor-Informed Motion Planning for Safe Autonomous Waterborne Navigation ⋆. *Submitted to TRA 2026 (under Review)*. https://www.seamless-project.eu/.

Lataire, E., Vantorre, M., & Delefortrie, G. (2018). The influence of the ship's speed and distance to an arbitrarily shaped bank on bank effects. *Journal of Offshore Mechanics and Arctic Engineering*, *140*(2), 21304.

Leveson, N., & Thomas, J. P. (2018). *Engineering a Safer World: Systems Thinking Applied to Safety*. MIT Press.

Li, J., Peng, Z., Liu, L., Wang, D., Wang, A., & Gu, N. (2023). Safety-Critical Line-of-Sight Path Following Guidance of an Under-Actuated Maritime Autonomous Surface Ship Based on Robust Optimization. *2023 42nd Chinese Control Conference (CCC)*, 2988–2993.

Liu, C., Negenborn, R. R., Chu, X., & Zheng, H. (2018). Predictive path following based on adaptive line-of-sight for underactuated autonomous surface vessels. *Journal of Marine Science and Technology (Japan)*, *23*(3), 483–494. https://doi.org/10.1007/s00773-017-0486-2

Liu, F., Shen, Y., He, B., Wang, D., Wan, J., Sha, Q., & Qin, P. (2019). Drift angle compensation-based adaptive line-of-sight path following for autonomous underwater vehicle. *Applied Ocean Research*, *93*, 101943.

Liu, X., & Zhang, W. (2024). Prescribed performance actuator-tolerance control for path following of unmanned surface vessels via the triggered adaptive line-of-sight guidance. *Computers and Electrical Engineering*, *120*, 109617.

Overheid.nl. (2025). *Binnenvaartpolitiereglement*. https://wetten.overheid.nl/BWBR0003628/2025-01-01

Park, B. S., & Yoo, S. J. (2016). Fault detection and accommodation of saturated actuators for underactuated surface vessels in the presence of nonlinear uncertainties. *Nonlinear Dynamics*, *85*(2), 1067–1077.

Pratson, L. F. (2023). Assessing impacts to maritime shipping from marine chokepoint closures. *Communications in Transportation Research*, *3*. https://doi.org/10.1016/j.commtr.2022.100083

Rogne, R. H., Johansen, T. A., & Fossen, T. I. (2014). Observer and IMU-based Detection and Isolation of Faults in Position Reference Systems and Gyrocompasses with Dual Redundancy in Dynamic Positioning. *2014 IEEE Conference on Control Applications (CCA)*, 83–88.

Rothmund, S. V. (2023). *Risk Awareness and Control of Autonomous Robots Sverre Velten Rothmund*. Norwegian University of Science and Technology.

Smeds, E., & Cavoli, C. (2021). *Pathways for accelerating transitions towards sustainable mobility in European cities*. Barcelona Centre for International Affairs (CIDOB).

Funded by the European Union

Funded by the European Union. Views and opinions expressed are however those of the author(s) only and do not necessarily reflect those of the European Union or CINEA. Neither the European Union nor CINEA can be held responsible for them. Grant Agreement N° 101096923.

Su, Y., Wan, L., Zhang, D., & Huang, F. (2021). An improved adaptive integral line-of-sight guidance law for unmanned surface vehicles with uncertainties. *Applied Ocean Research*, *108*, 102488.

Thieme, C. A., Rokseth, B., & Utne, I. B. (2023). Risk-informed control systems for improved operational performance and decision-making. *Proceedings of the Institution of Mechanical Engineers, Part O: Journal of Risk and Reliability*, *237*(2), 332–354.

Tran, H. A., Johansen, T. A., & Negenborn, R. R. (2023). Collision avoidance of autonomous ships in inland waterways - A survey and open research problems. *Journal of Physics: Conference Series*, *2618*(1). https://doi.org/10.1088/1742-6596/2618/1/012004

Tsolakis, A., Ferranti, L., & Reppa, V. (2024a). Active Thruster Fault Diagnosis for an Overactuated Autonomous Surface Vessel. *IFAC-PapersOnLine*, *58*(4), 43–48. https://doi.org/10.1016/j.ifacol.2024.07.191

Tsolakis, A., Ferranti, L., & Reppa, V. (2024b, November 5). Set-Membership Estimation for Fault Diagnosis of Nonlinear Systems. *Proceedings of the European Control Conference (ECC) 2025*. http://arxiv.org/abs/2411.03011

Tsolakis, A., Negenborn, R. R., Reppa, V., & Ferranti, L. (2024). Model Predictive Trajectory Optimization and Control for Autonomous Surface Vessels Considering Traffic Rules. *IEEE Transactions on Intelligent Transportation Systems*, *25*(8), 9895–9908. https://doi.org/10.1109/TITS.2024.3357284

Utne, I. B., Brurok, T., & Relling, T. (2020). Supervisory risk control for autonomous ships. *Safety and Reliability – Safe Societies in a Changing World*, 1535–1542.

Vantorre, M., Verzhbitskaya, E., & Laforce, E. (2002). Model test based formulations of ship-ship interaction forces. *Ship Technology Research*, *49*(3), 124–141.

Wróbel, K., Montewka, J., & Kujala, P. (2018). Towards the development of a system-theoretic model for safety assessment of autonomous merchant vessels. *Reliability Engineering & System Safety*, *178*, 209–224.

Wu, S., Ye, H., Liu, W., Yang, X., Liu, Z., & Zhang, H. (2024). An Improved ELOS Guidance Law for Path Following of Underactuated Unmanned Surface Vehicles. *Sensors*, *24*(16), 5384.

Yang, T., Han, C., Qin, M., & Huang, C. (2019). Learning-aided intelligent cooperative collision avoidance mechanism in dynamic vessel networks. *IEEE Transactions on Cognitive Communications and Networking*, *6*(1), 74–82.

Yoshioka, H., & Hashimoto, H. (2022). AI-based Collision Avoidance for Automatic Ship Navigation. *Proceedings of the 18th International Ship Stability Workshop*, 229–234.

Yoshioka, H., Hashimoto, H., & Matsuda, A. (2024). Artificial Intelligence for Cooperative Collision Avoidance of Ships Developed by Multi-Agent Deep Reinforcement Learning. *International Conference on Offshore Mechanics and Arctic Engineering*, *87844*, V006T08A036.

Funded by the European Union

Funded by the European Union. Views and opinions expressed are however those of the author(s) only and do not necessarily reflect those of the European Union or CINEA. Neither the European Union nor CINEA can be held responsible for them. Grant Agreement N° 101096923.

Zhang, C., Dhyani, A., Ringsberg, J. W., Thies, F., Negenborn, R. R., & Reppa, V. (2025). Nonlinear model predictive control for path following of autonomous inland vessels in confined waterways. *Ocean Engineering*, *334*, 121592.

Zhang, Q., Zhang, X., Zhu, B., & Reppa, V. (2021). Fault Tolerant Control for Autonomous Surface Vehicles via Model Reference Reinforcement Learning. *Proceedings of the IEEE Conference on Decision and Control*, *2021-December*, 1536–1541. https://doi.org/10.1109/CDC45484.2021.9683461

Zhao, X., He, Y., Huang, L., Mou, J., Zhang, K., & Liu, X. (2022). Intelligent Collision Avoidance Method for Ships Based on COLRGEs and Improved Velocity Obstacle Algorithm. *Applied Sciences (Switzerland)*, *12*(18). https://doi.org/10.3390/app12188926

Zhou, H., Ren, Z., Marley, M., & Skjetne, R. (2022). A guidance and maneuvering control system design with anti-collision using stream functions with vortex flows for autonomous marine vessels. *IEEE Transactions on Control Systems Technology*, *30*(6), 2630–2645.

Funded by the European Union

Funded by the European Union. Views and opinions expressed are however those of the author(s) only and do not necessarily reflect those of the European Union or CINEA. Neither the European Union nor CINEA can be held responsible for them. Grant Agreement N° 101096923.